

Can room temperature data for tunneling molecular junctions be analyzed within a theoretical framework assuming zero temperature?

Ioan Bâldea ^{a*}

Routinely, experiments on tunneling molecular junctions report values of conductances (G_{RT}) and currents (I_{RT}) measured at room temperature. On the other side, theoretical approaches based on simplified models provide analytic formulas for the conductance (G_{0K}) and current (I_{0K}) valid at zero temperature. Therefore, interrogating the applicability of the theoretical results deduced in the zero temperature limit to real experimental situations at room temperature (i.e., $G_{RT} \approx G_{0K}$ and $I_{RT} \approx I_{0K}$) is a relevant aspect. Quantifying the pertaining temperature impact on the transport properties computed within the ubiquitous single level model with Lorentzian transmission is the specific aim of the present work. Comprehensive results are presented for broad ranges of the relevant parameters (level's energy offset ϵ_0 and width Γ_a , and applied bias V) that safely cover values characterizing currently fabricated junctions. They demonstrate that the strongest thermal effects occur at biases below resonance ($2|\epsilon_0| - \delta\epsilon_0 \lesssim |eV| \lesssim 2|\epsilon_0|$). At fixed V , they affect an ϵ_0 -range whose largest width $\delta\epsilon_0$ is about nine times larger than the thermal energy ($\delta\epsilon_0 \approx 3\pi k_B T$) at $\Gamma_a \rightarrow 0$. The numerous figures included aim at conveying a quick overview on the applicability of the zero temperature limit to a specific real junction. In quantitative terms, the conditions of applicability are expressed as mathematical inequalities involving elementary functions. They constitute the basis of an interactive data fitting procedure proposed, which aims at guiding experimentalists interested in data processing in a specific case.

Keywords: molecular electronics, nanojunctions, single level model, thermal effects

1 Introduction

Routinely, charge transport experiments on molecular junctions are carried out at room temperature (RT). Nevertheless, most theoretical approaches—especially those based on model simulations^{1–5}—were developed for zero temperature ($T = 0$). In fact, a series of studies conducted at variable temperature (T)^{6–22} revealed a significant T -dependence of transport properties, which turned out to be fully compatible with a tunneling mechanism^{6,17,23–25}.

In this vein, interrogating the applicability of the theoretical results deduced in the zero temperature limit to real experimental situations at room temperature is a relevant aspect. Quantifying the pertaining thermal corrections to transport properties both at low bias (ohmic regime) and higher bias (nonlinear regime) is the aim of the present paper.

Although extensive numerical results will be reported below, this theoretical study is not merely intended to be a comprehensive numerical simulation experiment. Equally important, we aim at (i) clearly formulating simple conditions (mathematical inequalities) legitimating the applicability of formulas deduced theoretically for $T = 0$ to process transport measurements performed at room temperature and (ii) at proposing a practical receipt guiding experimentalists through an interactive data fitting procedure able to extract reliable model parameters.

2 Model and working equations

In order to make the paper self-contained, let us start with a short recap²⁶. Important insight into charge transport through tunneling molecular junctions can be gained by assuming a single dominant molecular orbital MO (usually, HOMO or LUMO) coupled via energy independent couplings $\Gamma_{s,t}$ to wide, flat metallic electrodes (hence Lorentzian-shaped transmission) subject to an applied bias V ^{2,3,5,27–30}.

The exact expression of the tunneling current for this single level model can be written as a particular case of the general formula deduced for the charge transport by tunneling³¹

$$\begin{aligned} I_{exact} &= \frac{2e}{h} \int_{-\infty}^{\infty} \mathcal{T}(\epsilon) \left[f\left(\epsilon - \frac{eV}{2}\right) - f\left(\epsilon + \frac{eV}{2}\right) \right] d\epsilon \\ &= \frac{2e}{h} \Gamma_s^2 \int_{-\infty}^{\infty} \frac{f(\epsilon - eV/2) - f(\epsilon + eV/2)}{(\epsilon - \epsilon_0)^2 + \Gamma_a^2} d\epsilon \quad (1) \end{aligned}$$

Above, $\epsilon_0 \equiv E_{MO} - E_F$ is the MO energy offset relative to electrodes' Fermi energy, $f(\epsilon) = 1/[1 + \exp(\beta\epsilon)]$ is the Fermi distribution ($1/\beta = k_B T$). Γ_g and Γ_a are the geometric and arithmetic MO-electrode couplings

$$\Gamma_g = \sqrt{\Gamma_s \Gamma_t} \quad (2a)$$

$$\Gamma_a = (\Gamma_s + \Gamma_t)/2 \quad (2b)$$

In general, the energy offset entering above is bias dependent, e.g.,^{5,32} $\epsilon_0 \rightarrow \epsilon_0(V) = \epsilon_0(V)|_{V=0} + \gamma eV$. A nonvanishing γ yields an asymmetric current voltage curve ($I(-V) \neq$

^a Theoretical Chemistry, Heidelberg University, Im Neuenheimer Feld 229, D-69120 Heidelberg, Germany

* E-mail: ioan.baldea@pci.uni-heidelberg.de

$-I(V)$). Although the formulas for the current (eqn (1), (3), and (9)) hold for arbitrary bias dependent MO offsets, given the fact that current rectification is not our main focus here, below we only present numerical results for a bias independent ε_0 ($\gamma \equiv 0$).

For MO's symmetrically coupled to electrodes, all Γ 's are equal: $\Gamma_a = \Gamma_g = \Gamma_s = \Gamma_r$. To avoid confusions (see ref. 26), we note that Γ 's used by us differ by a factor two from quantities denoted by the same symbol by other authors (e.g., ref. 30).

The expression of the current at zero temperature I_{0K} follows as an exact result from eqn (1) wherein the Fermi distribution $f(\varepsilon)$ reduces to the Heaviside step function^{2,3,5,27-30}

$$I_{0K} = \frac{2e}{h\Gamma_a} \Gamma_g^2 \left(\tan^{-1} \frac{\varepsilon_0 + eV/2}{\Gamma_a} - \tan^{-1} \frac{\varepsilon_0 - eV/2}{\Gamma_a} \right) \quad (3)$$

Because the zero bias (also referred to as ohmic or low bias) conductance defined by

$$G = \lim_{V \rightarrow 0} I(V)/V = \lim_{V \rightarrow 0} \partial I(V)/\partial V \quad (4)$$

represents the focus of most experiments done in molecular electronics, it is meaningful to consider the expression of G pertaining to the currents expressed by eqn (1) and (3). Eqn (3) straightforwardly yields

$$\frac{G}{G_0} \simeq \frac{G_{0K}}{G_0} = \frac{\Gamma_g^2}{\varepsilon_0^2 + \Gamma_a^2} \quad (5)$$

Sommerfeld expansions^{33,34} were employed to derive thermal corrections to G in closed analytic form^{24,25}. Although they may suffice for the present paper, wherein we aim at considering rather modest deviations of transport properties at room temperature from those at $T = 0$, we prefer to use the zero bias (ohmic) value of the exact conductance pertaining to the exact current I_{exact} , because it can be expressed analytically for arbitrary values of the model parameters²⁴. In terms of the real part of Euler's trigamma function of complex argument function $\psi'(z)$ ^{35,36}, the exact conductance reads

$$\frac{G_{exact}}{G_0} = \frac{\Gamma_g^2}{2\pi\Gamma_a k_B T} \text{Re} \psi' \left(\frac{1}{2} + \frac{\Gamma_a}{2\pi k_B T} + i \frac{\varepsilon_0}{2\pi k_B T} \right) \quad (6)$$

The trigamma function represents the derivative of the digamma function, $\psi'(z) \equiv \psi(1; z) \equiv \frac{d}{dz} \psi(z)$, which, in turn, is the logarithmic derivative of Euler's gamma function³⁶.

In view of the foregoing analysis, situations wherein I_{0K} (eqn (3)) and G_{0K} (eqn (5)) represent good approximation of I_{exact} (eqn (1)) and G_{exact} (eqn (6)), respectively can be referred to as the low temperature limit

$$\text{Low temperature limit: } \begin{cases} I_{0K} \approx I_{exact} \\ G_{0K} \approx G_{exact} \end{cases} \quad (7)$$

The low temperature limit applies in cases where the transmission function (whose shape is controlled by ε_0 and Γ_a) exhibits a negligible variation within energy ranges of widths of the order $\sim k_B T$ around the electrode Fermi levels ($\pm eV/2$). Consequently, MO levels need be sufficiently far away from the Fermi levels for the low temperature limit to apply; $||\varepsilon_0| - |eV|/2|$ should be sufficiently larger than $k_B T$.

Provided that the arguments of the inverse trigonometric functions entering eqn (3) are sufficiently large ($x > x_0 = 2.928$, see Fig. S1)

$$x \equiv \frac{|\varepsilon_0| - |eV|/2}{\Gamma_a} > x_0 = 2.928 \quad (8a)$$

$$\tan^{-1}(x) \simeq \frac{\pi}{2} - \frac{1}{x} \quad (8b)$$

eqn (3) reduces to^{5,26}

$$I_{0K, \text{off}} = G_0 \frac{\Gamma_g^2}{\varepsilon_0^2 - (eV/2)^2} V \quad (9)$$

where $G_0 = 2e^2/h = 77.48 \mu\text{S}$ is the universal conductance quantum.

As a rule of thumb, for applying eqn (9) we suggested (see ref. 26 and citations therein) an upper bias limit

$$|V| \lesssim V_{1.4} \equiv 1.4 |\varepsilon_0|/e \quad (10)$$

Eqn (10) is justified by the the fact that most molecular junctions have a conductance much smaller than G_0

$$G/G_0 \lesssim 0.01 \xrightarrow{\Gamma_g \approx \Gamma_a} \Gamma_a \lesssim |\varepsilon_0|/10 \quad (11)$$

In cases where eqn (11) holds, eqn (10) follows via eqn (8a).

Eqn (10) and (11) express the rationale of using the term "off-resonant single level model" for the transport by tunneling modeled using eqn (9): at the biases envisaged (eqn (10)), the energy mismatch between (MO) level and the closest electrodes' electrochemical potential ($|\varepsilon_0| \gtrsim 0.7|eV|$ versus $|eV|/2$ is much larger than the level broadening Γ_a due to the MO-coupling to electrodes ($|\varepsilon_0| - |eV|/2 \gg \Gamma_a$).

Eqn (9) straightforwardly yields

$$\frac{G}{G_0} \simeq \frac{G_{0K, \text{off}}}{G_0} = \frac{\Gamma_g^2}{\varepsilon_0^2} \quad (12)$$

For large values of the argument in the RHS of eqn (6)

$$|z| \equiv \sqrt{\left(\frac{1}{2} + \frac{\Gamma_a}{2\pi k_B T} \right)^2 + \left(\frac{\varepsilon_0}{2\pi k_B T} \right)^2} \gg 1, \quad |\arg z| < \pi$$

the trigamma function can be approximated by the first term of its asymptotic expansion³⁶

$$\psi'(z) = \frac{1}{z} + \mathcal{O}(z^{-2})$$

This shows that the exact eqn (6) of the zero bias conductance G_{exact} recovers the expression of G_{0K} at $T = 0$ (eqn (5)) in the (low temperature) limit

$$\sqrt{(\pi k_B T + \Gamma_a)^2 + \varepsilon_0^2} \gg 2\pi k_B T$$

The above equation has a precise physical content: thermal effects do not substantially affect the charge transport in cases where the transmission function does not appreciably varies at energies accessed by electrons thermally excited above electrode's Fermi energy. It expresses the low temperature condition at $V = 0$ but the physical insight gained in this way is clear and this makes generalization at $V \neq 0$ straightforward.

At finite biases ($V \neq 0$), the low temperature limit is justified in situations where energy ranges around ϵ_0 having widths $\sim \Gamma_a$ (wherein the transmission function rapidly varies) do not notably overlap with energy ranges around electrodes' electrochemical potential smeared out by thermic excitations. An applied bias brings the MO closer in energy to the closest electrode's electrochemical potential. Mathematically, this amounts to replace in the above equation ϵ_0 by $|\epsilon_0| - |eV|/2$

$$\sqrt{(\pi k_B T + \Gamma_a)^2 + (|\epsilon_0| - |eV|/2)^2} \gg 2\pi k_B T \quad (13a)$$

or, equivalently,

$$\sqrt{(\pi k_B T + \Gamma_a)^2 + (|\epsilon_0| - |eV|/2)^2} > q\pi k_B T \quad (13b)$$

where q is a dimensionless number sufficiently larger than two.

To sum up, while the foregoing analysis allows one to understand that the applicability of the zero temperature limit can be expressed in terms of certain mathematical inequalities, what does "sufficiently small" or "sufficiently large" precisely mean in the foregoing analysis is a question that cannot merely be settled based on qualitative considerations like those delineated above.

To address this question and find out, e.g., what is a "good" numerical value of q to be used in eqn (13b), we conducted extensive numerical simulations, as detailed in the next section.

3 Results of numerical simulations

The impact of a variable temperature on the charge transport by tunneling is an interesting topic (see, e.g., the Arrhenius-Sommerfeld transition³⁷ or the possibility of estimating the number of molecules in large area molecular junctions²⁵), but a full analysis of thermal effects at variable temperature will not be attempted here. Rather, in view of unpleasant flaws in recent analysis of the thermal effects (see discussion in ref. 26), we find it useful and aim at comprehensively characterizing physical situations wherein transport properties at room temperature can be reasonably estimated via more facile computations assuming $T = 0$. Therefore, in all numerical results presented below, "temperature" means "room temperature" (RT, $T = T_{RT} = 298.15$ K, $k_B T = k_B T_{RT} = 25.7$ meV). "Exact" current and zero bias conductance values are values at room temperature: $I_{exact} = I_{RT}$ and $G_{exact} = G_{RT}$.

The results reported below quantify the impact of the three parameters which are relevant for the present study: ϵ_0 , Γ_a , and V . Noteworthy, Γ_g plays no role in discussing relative deviations between the cases $T = 0$ and RT; it merely enters all above formulas for G 's and I 's as a multiplicative factor. The broad ranges of model parameters ϵ_0 and Γ_a considered safely cover experimentally estimated values for real molecular junctions^{21,29,38-46}.

A nonvanishing temperature has an insignificant effect on the resonant current. Results for this case ($eV = 2\epsilon_0$) depicted in Fig. S11a reveal a slight current reduction ($I_{RT} < I_{0K}$) limited a very narrow range ($\epsilon_0 = eV/2 \lesssim k_B T$).

A significant impact on the current occurs only slightly away from strict resonance but not strictly on resonance ($\epsilon_0 = eV/2$). In general, the impact is qualitatively different, depending on whether the energy level lies outside or within the Fermi window ($|\epsilon_0| > |eV|/2$ or $|\epsilon_0| < |eV|/2$, respectively). Indeed, as visualized in Fig. S3, except for very small values of ϵ_0 (cf. Fig. S4), thermal effects enhance the current ($I_{RT} > I_{0K}$) in the former case while diminishing it ($I_{RT} < I_{0K}$) in the latter case. Because $|\epsilon_0| = |eV|/2$ corresponds to resonant tunneling (MO energy equal to the electrochemical potential of one electrode), biases for which $|\epsilon_0| > |eV|/2$ will be referred to as "below resonance", while those for which $|\epsilon_0| < |eV|/2$ will be referred to as "above resonance".

Before proceeding with specific results, we make two remarks to clarify why the various figures presented below contain white (empty) regions.

First, the various figures that follow comprise one panel depicting positive values of the relative deviations (always in percent) $I_{RT}/I_{0K} - 1 (> 0)$ for situations below resonance ($|\epsilon_0| > |eV|/2$), and another panel depicting values of $I_{0K}/I_{RT} - 1 (> 0)$ for situations above resonance ($|\epsilon_0| < |eV|/2$). However, in order to convey an overall picture, both of these panels depict the full ranges of V or ϵ_0 (i.e., both below resonance and above resonance). For this reason, e.g., the left (right) part of the panels depicting "above resonance" ("below resonance") situations at fixed ϵ_0 like those in Fig. 1a (Fig. 1b) is empty. (In the empty area of Fig. 1a $I_{RT}/I_{0K} - 1$ is negative; likewise, in the empty area of Fig. 1b $I_{0K}/I_{RT} - 1$ is also negative.) We think that this presentation is more expressive than that (mathematically equivalent) of Figs. S2a and S2c (or Figs. S2b and S2d) of the ESI[†], where situations where $I_{RT} > I_{0K}$ and $I_{RT} < I_{0K}$ (or $I_{RT} < I_{0K}$ and $I_{RT} > I_{0K}$, respectively) are depicted in the same panel.

Second, emphasis in this paper is on specifying situations wherein the zero temperature limit applies. Therefore, in the various figures shown below we will only depict parameter regions corresponding to "thermal corrections" (i.e., "reasonably weak" thermal effects), namely those wherein $|I_{0K}|/2 < |I_{RT}| < 2|I_{0K}|$. For this reason, situations wherein the relative deviations $I_{0K}/I_{RT} - 1$ or $I_{RT}/I_{0K} - 1$ exceed 100% appear as white (empty) regions in the various diagrams presented.

3.1 Thermal effects at fixed MO energy offset

Because the model with $\gamma \equiv 0$ possesses charge conjugation symmetry and all physical observables are invariant under an $\epsilon_0 \rightarrow -\epsilon_0$ transformation, in the presentation that follows we can and will restrict ourselves to positive values of ϵ_0 and V . Whenever confusion can be excluded, we will write ϵ_0 and V instead of $|\epsilon_0|$ and $|V|$.

Figs. 1 to 3 as well as Figs. S5 to S9 of the ESI[†] depict thermal effects for variable bias V at fixed values of the MO energy offset ϵ_0 .

In accord with the general considerations delineated in Sec. 2, these figures show that the current I_{0K} computed at $T = 0$ deviates from the current I_{RT} at room temperature for biases around the resonance value $eV = 2\epsilon_0$. Lowering of the MO offset from

the value $\epsilon_0 = 1$ eV (Fig. 1a) to $\epsilon_0 = 0.7; 0.5; 0.4; 0.3; 0.2; 0.1$ eV (Figs. S5a, S6a, 2a, S7a, S8a, and S9a, respectively) shifts the predominantly red region (corresponding to deviations up to 100%) from $V \lesssim 2$ V to bias ranges around the smaller values $V (= 2\epsilon_0/e) = 1.4; 1; 0.8; 0.6; 0.4; 0.2$ V.

To make more evident the fact that thermal effects are intimately related to the resonance condition ($eV \approx 2\epsilon_0$), Fig. 3 and Fig. S10 of the ESI[†] depict relative deviations of I_{0K} from I_{RT} computed for various MO offsets aligned to the same abscissa value (namely, $eV - 2\epsilon_0$). Figs. 3 and Figs. S11c and d make it clear that thermal effects around resonance ($|eV| \approx 2|\epsilon_0|$) are insensitive to ϵ_0 provided that the latter is reasonably large with respect to the thermic energy $k_B T = 25.7$ meV. Loosely speaking, this means $\epsilon_0 \gtrsim 0.4$ eV. At smaller values of ϵ_0 , slightly broader parameter areas are affected, which extend towards larger values of Γ_a (Fig. S10).

In all cases, temperature's impact above resonance ($V > 2\epsilon_0/e$) is weaker than below resonance. Most significantly affected is the bias range below resonance

$$\max(2\epsilon_0/e - \delta V(\Gamma_a), 0) \lesssim V < 2\epsilon_0/e, \delta V(\Gamma_a) < \delta V|_{\Gamma_a \rightarrow 0} \quad (14a)$$

whose width $\delta V \equiv \delta V(\Gamma_a)$ is nearly independent of ϵ_0 . At small Γ_a , it amounts to

$$\delta V|_{\Gamma_a \rightarrow 0} \approx 0.5 \text{ V} \quad (14b)$$

Moving upwards to larger values of Γ_a , the bias range δV where thermal effects are significant becomes gradually narrower.

Along with deviations with respect to the exact current I_{RT} at room temperature of the current I_{0K} computed at $T = 0$ (Figs. 1a and 2a as well as Figs. S5a to S9a of the ESI[†]), in Figs. 1b and 2b as well as in Figs. S5a to S9b of the ESI[†] we also show deviations from I_{RT} of the current $I_{0K,off}$ computed via eqn (9). Inspection of these figures reveals that, for biases V sufficiently below resonance and sufficiently large MO energy offsets ($\epsilon_0 \gtrsim 0.4$ eV; noteworthy, the same numerical value as encountered above in the analysis based on eqn (3)), eqn (9) is very accurate irrespective of the value of Γ_a .

Always in the bias range compatible with eqn (10), deviations of $I_{0K,off}$ from I_{RT} become progressively significant as ϵ_0 decreases below $\epsilon_0 \lesssim 0.4$ eV (Figs. 2b and S7b to S9b). Still, even in such situations, the approximation $I_{0K,off} \approx I_{RT}$ is as good as the approximation $I_{0K} \approx I_{RT}$ as long as Γ_a is sufficiently small to comply with eqn (11); compare among themselves panels (b) and (c) in Figs. 2 and S9, and in Figs. S7 to S9 of the ESI[†].

3.2 Thermal effects at fixed bias voltage

Complementary to the presentation in Sec. 3.1, in Figs. 4 to 6 and Figs. S12 to S14 of the ESI[†] we next show results depicting room temperature effects in the plane (ϵ_0, Γ_a) for several values of the bias ranging from the upper limit of biases which real molecular junctions can withstand ($V = 1.5$ V) down to low biases ($V = 0.1$ V) typically chosen to experimentally estimate the “zero-bias” conductance; see Figs. 4 and 6, and Figs. S12 to S14.

Again, these figures show that the current I_{0K} computed at $T = 0$ deviates from the current at room temperature for energy offsets around the resonance value $\epsilon_0 \approx eV/2$. Basically, Figs. 4a and 5a, and S12a and S13a depict changes expected in view of the above considerations; lowering the bias $V = 1.5; 1.0; 0.5; 0.1$ V shifts the

predominantly red region in these figures (corresponding to deviations up to 100%) to the smaller ϵ_0 around the values $\epsilon_0 (= eV/2) = 0.75; 0.5; 0.25; 0.05$ eV.

To emphasize again the fact that current's thermal enhancement is directly related to the resonance condition ($\epsilon_0 \approx eV/2$), we depicted in Fig. S10 relative deviations of I_{0K} from I_{RT} computed for various biases aligned to the same abscissa value ($\epsilon_0 = eV/2$). Fig. S10 makes it clear that thermal effects around resonance ($\epsilon_0 \approx eV/2$) are insensitive to V , provided that the corresponding energy is reasonably large with respect to the thermic energy $k_B T$. Consistent to Sec. 3.1, thermal effects appear to be weaker above resonance ($\epsilon_0 < 2eV$) than below resonance, where they are pronounced in the range

$$eV/2 < \epsilon_0 \lesssim eV/2 + \delta\epsilon_0(\Gamma_a) \\ \delta\epsilon_0(\Gamma_a) < \delta\epsilon_0|_{\Gamma_a \rightarrow 0} \approx 0.25 \text{ eV} \approx 3\pi k_B T_{RT} \quad (15)$$

Consistent with Sec. 3.1 and eqn (14), $\delta\epsilon_0(\Gamma_a) \approx e\delta V(\Gamma_a)/2$ is seen to be nearly independent of V . Its value at small Γ_a is $\delta\epsilon_0|_{\Gamma_a \rightarrow 0} \approx e\delta V|_{\Gamma_a \rightarrow 0}/2 \approx 0.25$ eV and decreases as Γ_a becomes larger.

Along with deviations with respect to the exact current I_{RT} at room temperature of the current I_{0K} computed at $T = 0$ (Figs. 4a, S12a, 5a, and S13a), in Figs. 4b, S12b, 5b, and S13b we also show deviations of current $I_{0K,off}$ computed via eqn (9). Inspection of the aforementioned figures reveals that, in the range compatible with eqn (10) and (11), it is very accurate. At $V = 0.5$ V, deviations of $I_{0K,off}$ from I_{RT} are significant only for model parameter values where deviations of I_{0K} from I_{RT} are also significant. This fact is understandable: being a limiting case of eqn (3), eqn (9) cannot be expected to perform better than eqn (3). $I_{0K,off}$ is less accurate than I_{0K} only for values of the parameters violating the conditions assumed in the deduction of eqn (9). This is the case of the upper left corner of Fig. S13b, wherein the small values of ϵ_0 and the large values of Γ_a are incompatible with eqn (11).

3.3 Thermal effects on the zero bias conductance

As an important case of a fixed value of V (namely, $V \rightarrow 0$), in Fig. 7 we depict deviations of the zero temperature values G_{0K} and $G_{0K,off}$ (eqn (5) and (12), respectively) from the exact conductance $G_{exact} = G_{RT}$ (eqn (6)).

In agreement with eqn (15) at $V = 0$, significant departures of G_{0K} from G_{RT} occur in the range

$$\epsilon_0 < \delta\epsilon_0(\Gamma_a) < \delta\epsilon_0|_{\Gamma_a \rightarrow 0} \approx 0.25 \text{ eV} \approx 3\pi k_B T_{RT} \quad (16)$$

whose width is the largest at $\Gamma_a \rightarrow 0$ ($\delta\epsilon_0|_{\Gamma_a \rightarrow 0} \approx 0.25$ eV) and becomes smaller as Γ_a increases (Fig. 7a). As for $G_{0K,off}$, confirming the analysis of Sec. 2, it is as accurate as G_{0K} unless the condition $\Gamma_a \ll \epsilon_0$ is violated (cf. eqn (5) and (12); see the upper left corner of Fig. 7b).

3.4 An experimental digression

To illustrate the above ideas with specific examples from real molecular electronics, we will consider in this section three molecular junctions fabricated using different platforms: single molecule junctions of 4,4'-bisnitrotolane (BNT) and gold electrodes fabricated using mechanically controlled break junction technique²⁹, CP-AFM

junctions fabricated with perylene tetracarboxylic acid diimide (PDI) molecules and silver electrodes²¹, and large area junctions with EGaIn electrodes based on molecules of alkanethiolates functionalized with a ferrocene (Fc) unit¹⁷.

What these junctions have in common is their comparable, small MO energy offset: $\epsilon_0 \simeq 0.27 \text{ eV}$ ²⁹, 0.26 eV ²¹, and 0.24 eV ²⁵, respectively. What makes the first junction different from the last two is the MO width: $\Gamma_a \simeq 35 \text{ meV}$ ²⁹ much larger than $\Gamma_a \simeq 6 \text{ meV}$ ²¹ and 4.6 meV ²⁵, respectively.

In Fig. 8 we used the above parameter values to simulate I - V “measurements” (represented as red points) by overimposing a bit disorder on the values of the current calculated via eqn (1) at $T = 298.15 \text{ K}$. Re-fitting for self-consistency these “experimental” I - V data using eqn (1) yielded the curves for I_{RT} depicted by blue lines in Fig. 8.

The curves for I_{0K} and $I_{0K,off}$ computed using eqn (3) and (9) and the same parameter values are depicted by the light green and dark green lines, respectively. The difference between these curves (assuming $T = 0$) and the red curves (assuming $T = 298.15 \text{ K}$) is a temperature effect. Given the large value of $\Gamma_a (= 35 \text{ meV})$, notwithstanding the small value of ϵ_0 , this effect is weak for BNT (Figs. 8a and d). The temperature effect is considerably more pronounced for the PDI junction having $\Gamma_a = 6 \text{ meV}$ (cf. Figs. 8b and e). In agreement with Figs. 8f, the thermal corrections $I_{RT}/I_{0K} - 1$ exceeding 100% at $V = 0.4 \text{ V}$ and $V = 0.3 \text{ V}$ lie in the empty (white) region in Figs. S14a and b. The smaller values $\epsilon_0 \simeq 0.24 \text{ eV}$ versus $\epsilon_0 \simeq 0.26 \text{ eV}$ and $\Gamma_a = 6 \text{ meV}$ versus $\Gamma_a = 4.6 \text{ meV}$ make the temperature effect in the Fc-based junction (Figs. 8c and f) even stronger than for PDI. In the former case, the thermal corrections $I_{RT}/I_{0K} - 1$ exceed 100% not only at $V = 0.4 \text{ V}$ and $V = 0.3 \text{ V}$ but also at the lower bias $V = 0.2 \text{ V}$ (cf. Figs. 8c and f and the empty (white) region in Figs. S14a to c).

4 Applicability of the zero temperature approaches expressed by analytic inequalities

The numerical results reported above allow us to indicate (more precisely than done in Sec. 2) the parameter ranges where transport measurements performed at room temperature can be accurately analyzed using analytic formulas valid for $T = 0$, which are more convenient for experimental data processing than those for $T \neq 0$.

As anticipated in Sec. 2 and confirmed by the foregoing numerical simulations (Sec. 3), the strongest thermal effects occur below resonance ($|eV| < 2|\epsilon_0|$). Therefore, the analysis in this section will focus on such situations.

4.1 $I_{0K} \approx I_{RT}$. Applicability of eqn (3)

Corroborating the general considerations that led to eqn (13) with the specific results expressed by eqn (14) and (15), we arrive at concluding that the value of q “sufficiently” larger than two (cf. Sec. 2) needs in fact not be very large. Namely, to ensure that the description based on I_{0K} is accurate (i.e., $I_{0K} \simeq I_{RT}$), it is sufficient to set $q = 3$. The highest bias at which eqn (3) applies is defined by the

value $V_{max}^{0K} (< 2|\epsilon_0|/e)$ indicated below

$$\sqrt{(\pi k_B T + \Gamma_a)^2 + (|\epsilon_0| - eV_{max}^{0K}/2)^2} = 3\pi k_B T \quad (17a)$$

The diagram of $V_{max}^{0K} = V_{max}^{0K}(\epsilon_0, \Gamma_a)|_{q=3}$ is depicted in Fig. 9a while the pertaining thermal corrections for current (not exceeding a few percent for most realistic parameters) are shown in Fig. 9b. Imposing larger values of q (e.g., $q = 3.5$, Fig. S17 or $q = 4$, Fig. S18) does not significantly decrease the thermal corrections while artificially decreasing V_{max}^{0K} .

Notice that only values $\epsilon_0 > \epsilon_0^{min}$ larger than a certain minimum value are shown in Fig. 9. This expresses the physical reality that, irrespective of bias ($eV < 2\epsilon_0$), the low temperature limit does not apply for too small values of ϵ_0 . The smallest value ϵ_0^{min} , estimated by setting $q = 3$ in eqn (13b),

$$|\epsilon_0| > \epsilon_0^{min} = \sqrt{(3\pi k_B T)^2 - (\pi k_B T + \Gamma_a)^2} \quad (17b)$$

very weakly depends on Γ_a . It is visualized by the line separating the white and colored portions in Fig. 9.

Eqn (13a) also makes it clear that, irrespective of the values of ϵ_0 and V , the low temperature limit applies for Γ_a “sufficiently” larger than $k_B T$. Inspection of the previously analyzed figures reveals that, in fact, Γ_a needs not be much larger than $k_B T (= 25.7 \text{ meV})$. The low temperature limit $I_{RT} \approx I_{0K}$, $G_{RT} \approx G_{0K}$ is reasonably accurate at the largest value ($\Gamma_a = 50 \text{ meV}$) shown in those figures. Depicting values of the ratio I_{0K}/I_{RT} close to unity both for $\Gamma_a = 50 \text{ meV}$ and for $\Gamma_a = \pi k_B T_{RT} = 80.7 \text{ meV}$, Fig. S16 additionally emphasizes this aspect.

To sum up, eqn (3) is applicable for biases $|V|$ smaller than V_{max}^{0K} (eqn (17a)) and $|\epsilon_0|$ larger than ϵ_0^{min} (eqn (17b)).

4.2 $I_{0K,off} \approx I_{RT}$. Applicability of eqn (9)

Let us now discuss the applicability of eqn (9). As re-emphasized recently²⁶, this equation should be applied only for biases sufficiently below resonance⁵. Eqn (9) should by no means be applied above resonance ($|eV| \geq 2|\epsilon_0|$) where the denominator becomes negative and, completely nonphysically, current and bias would have opposite directions²⁶.

Derived as a limiting case of eqn (3)⁵, eqn (9) is implicitly subject to the low temperature restrictions expressed by eqn (17). In addition, the highest bias to which eqn (9) applies has to satisfy eqn (8a), that is

$$|V| < V_{max}^{off}; eV_{max}^{off} < 2|\epsilon_0| - 5.856\Gamma_a (< 2|\epsilon_0|/e) \quad (18a)$$

The above condition ensures that $I_{0K,off}$ does not differ from I_{0K} by more than 2% (Fig. S1). Corroborating with (eqn (17a)), this yields the highest bias at which eqn (9) is accurate

$$|V| < V_{max}^{0K,off} \equiv \min(V_{max}^{0K}, V_{max}^{off}) \quad (18b)$$

Diagrams for $V_{max}^{0K,off}$ along with the current deviations $I_{0K,off}/I_{RT} - 1$ at this bias ($V = V_{max}^{0K,off}$) are depicted in panels c and d of Figs. 9, S17, and S18. Notice the very close similarity of these panels (relying on $I_{0K,off}$) to panels a and b (relying on I_{0K}) of the same figures.

This confirms the analysis of Sec. 2. In off-resonance cases (which do represent the main focus of most experiments on molecular junctions), the description based on eqn (9) is essentially as good as that based on eqn (3) while applicable up to an upper bias which is basically the same.

To conclude, eqn (9) is accurate at biases $|V|$ smaller than $V_{max}^{0K,off}$ (eqn (18b)) and $|\epsilon_0|$ larger than ϵ_0^{min} (eqn (17b)).

4.3 Interactive data fitting using eqn (9)

The various figures presented above revealed that eqn (9) used for biases $|V| < V_{1.4}$ (eqn (10)) is reliable in broad area of the model parameters ϵ_0 and Γ_a . Therefore, we recommend to use this method first for I - V data fitting, as the fitting parameters ϵ_0 thus obtained were validated through additional ultraviolet photoelectron spectroscopy (UPS) studies on benchmark molecular junctions^{41,42,47}.

When we suggested $V_{1.4}$ of eqn (10) as upper bias for the applicability of eqn (9), we had in mind a pragmatic reason (see ref. 26 and citations therein): most molecular junctions currently fabricated possess a conductance $G/G_0 < \lesssim 0.01$ obeying eqn (11). Fig. S19a depicts parameter ranges wherein at $V = V_{1.4}$ $I_{0K,off} \approx I_{RT}$ holds within 10% (=“typical” experimental accuracy). The model parameters characterizing benchmark molecular junctions with alkyl⁴² and oligophenylene⁴¹ backbones deduced from data fitting using eqn (9) for biases $|V| < V_{1.4}$ fall in the parameter ranges depicted in Fig. S19a.

For junctions having a normalized conductance G/G_0 larger than 0.01, narrower bias ranges should be employed for reliably extracting the model parameters ϵ_0 and Γ_a from data fitting based on eqn (9).

Fig. S19 may help to illustrate this idea. Suppose we investigate a molecular junction having $\epsilon_0 = 0.5$ eV and $\Gamma_a = 1.5$ meV (obviously, values not known a priori) and can collect experimental I - V data in the range -0.7 V $< V < 0.7$ V. To exploit the full experimental information available, we use eqn (9) for data fitting in the entire range $V_{fit} = 0.7$ V, $-V_{fit} < V < V_{fit}$. This yields certain best fit parameters $\tilde{\epsilon}_0$ and $\tilde{\Gamma}_a$. We insert these parameter values in eqn (18b) and (17b) and compute $V_{max}^{0K,off} \rightarrow \tilde{V}_{max}^{0K,off}$ and $\epsilon_0^{min} \rightarrow \tilde{\epsilon}_0^{min}$. Because the point ($\epsilon_0 = 0.5$ eV, $\Gamma_a = 1.5$ meV) lies in the empty (white) part of the diagram in Fig. S19a depicted for $eV = 1.4\epsilon_0$, we will have to conclude that our values of V_{fit} and $\tilde{\epsilon}_0$ fail to satisfy at least one of the two conditions requested ($V_{fit} < V_{max}^{0K,off}$, $\tilde{\epsilon}_0 > \epsilon_0^{min}$). We narrow the fitting range and arrive (possibly after several trials and errors) at selecting the smaller value $V_{fit} = 0.5$ V. With the new best fit parameters $\tilde{\epsilon}_0 = 0.5$ eV and $\tilde{\Gamma}_a = 1.5$ meV and the new pertaining values $\tilde{V}_{max}^{0K,off}$ and $\tilde{\epsilon}_0^{min}$, we check that eqn (18b) and eqn (17b) are simultaneously satisfied. Indeed, the point ($\epsilon_0 = 0.5$ eV, $\Gamma_a = 1.5$ meV) belong to the “allowed” zone in Fig. S19b depicted for $\epsilon_0 = eV$.

5 Conclusion

Notwithstanding impressive computational facility currently available, experimentalists continue to prefer simple theoretical models to process the data they measure. Representing “by definition” a simplified description of the real world, a model cannot be blindly utilized ignoring the conditions of applicability. Theory should make these conditions as transparent as possible.

By combining insight gained from a qualitative analysis of the relevant equations with extensive numerical simulations, in the present we were able to provide the experimentalists not only with numerous diagrams wherein they can presumably identify the specific case of their interest, but also with simple mathematical inequalities that they can straightforwardly use to check whether processing transport data measured on molecular junctions at room temperature using a zero temperature formalism is adequate or not.

Irrespective whether or not the fitting curves acceptably reproduced the measured I - V traces, model parameters extracted by using eqn (3) for data fitting can be trusted only if they satisfy eqn (17a) and (17b). Likewise, model parameters extracted by using eqn (9) are reliable only if they obey eqn (18b) and (17b).

Should this be not the case, one can next try to obtain reliable parameters by gradually narrowing the bias range used for data fitting according to the interactive procedure described in Sec. 4.3. Should this attempt also fail, employing the less convenient eqn (1) is the last attempt to be done before concluding that either electron (or hole) tunneling does not occur via a single level (MO), that transmission is not Lorentzian²³, or that, e.g., hopping rather than tunneling is at work in the envisaged junction.

Acknowledgments

Financial support from the German Research Foundation (DFG Grant No. BA 1799/3-2) in the initial stage of this work and computational support by the state of Baden-Württemberg through bwHPC and the German Research Foundation through Grant No. INST 40/575-1 FUGG (bwUniCluster 2.0, bwForCluster/MLS&WISO 2.0/HELIX, and JUSTUS 2.0 cluster) are gratefully acknowledged.

Notes and references

- 1 W. Schmickler, *J. Electroanal. Chem.*, 1986, **204**, 31–43.
- 2 I. R. Peterson, D. Vuillaume and R. M. Metzger, *J. Phys. Chem. A*, 2001, **105**, 4702–4707.
- 3 C. A. Stafford, *Phys. Rev. Lett.*, 1996, **77**, 2770–2773.
- 4 M. Büttiker and D. Sánchez, *Phys. Rev. Lett.*, 2003, **90**, 119701.
- 5 I. Bâldea, *Phys. Rev. B*, 2012, **85**, 035442.
- 6 M. Poot, E. Osorio, K. O’Neill, J. M. Thijssen, D. Vanmaekelbergh, C. A. van Walree, L. W. Jenneskens and H. S. J. van der Zant, *Nano Lett.*, 2006, **6**, 1031–1035.
- 7 S. H. Choi, B. Kim and C. D. Frisbie, *Science*, 2008, **320**, 1482–1486.
- 8 H. Song, Y. Kim, Y. H. Jang, H. Jeong, M. A. Reed and T. Lee, *Nature*, 2009, **462**, 1039–1043.
- 9 I. Diez-Perez, J. Hihath, T. Hines, Z.-S. Wang, G. Zhou, K. Müllen and N. Tao, *Nat Nano*, 2011, **6**, 226–231.
- 10 G. Sedghi, V. M. Garcia-Suarez, L. J. Esdaile, H. L. Anderson, C. J. Lambert, S. Martin, D. Bethell, S. J. Higgins, M. Elliott, N. Bennett, J. E. Macdonald and R. J. Nichols, *Nat. Nanotechnol.*, 2011, **6**, 517–523.
- 11 R. Heimbuch, H. Wu, A. Kumar, B. Poelsema, P. Schön, G. J. Vancso and H. J. W. Zandvliet, *Phys. Rev. B*, 2012, **86**, 075456.
- 12 R. L. McCreery, H. Yan and A. J. Bergren, *Phys. Chem. Chem. Phys.*, 2013, **15**, 1065–1081.
- 13 K. Asadi, A. J. Kronemeijer, T. Cramer, L. Jan Anton Koster, P. W. M. Blom and D. M. de Leeuw, *Nat Commun*, 2013, **4**, 1710.
- 14 S. Saha, J. R. Owens, V. Meunier and K. M. Lewis, *Appl. Phys. Lett.*, 2013, **103**, 173101.

- 15 L. Xiang, T. Hines, J. L. Palma, X. Lu, V. Mujica, M. A. Ratner, G. Zhou and N. Tao, *J. Am. Chem. Soc.*, 2016, **138**, 679–687.
- 16 R. L. McCreery, *Beilstein J. Nanotechnol.*, 2016, **7**, 32–46.
- 17 A. R. Garrigues, L. Yuan, L. Wang, S. Singh, E. del Barco and C. A. Nijhuis, *Dalton Trans.*, 2016, **45**, 17153–17159.
- 18 K. S. Kumar, R. R. Pasula, S. Lim and C. A. Nijhuis, *Adv. Mater.*, 2016, **28**, 1824–1830.
- 19 N. Xin, C. Jia, J. Wang, S. Wang, M. Li, Y. Gong, G. Zhang, D. Zhu and X. Guo, *J. Phys. Chem. Lett.*, 2017, **8**, 2849–2854.
- 20 A. Morteza Najarian and R. L. McCreery, *ACS Nano*, 2017, **11**, 3542–3552.
- 21 C. E. Smith, Z. Xie, I. Bâldea and C. D. Frisbie, *Nanoscale*, 2018, **10**, 964–975.
- 22 N. Xin, C. Hu, H. Al Sabea, M. Zhang, C. Zhou, L. Meng, C. Jia, Y. Gong, Y. Li, G. Ke, X. He, P. Selvanathan, L. Norel, M. A. Ratner, Z. Liu, S. Xiao, S. Rigaut, H. Guo and X. Guo, *J. Am. Chem. Soc.*, 2021, **143**, 20811–20817.
- 23 I. Bâldea, *Phys. Chem. Chem. Phys.*, 2017, **19**, 11759 – 11770.
- 24 I. Bâldea, *Adv. Theor. Simul.*, 2022, **5**, 202200158.
- 25 I. Bâldea, *Int. J. Mol. Sci.*, 2022, **23**, 14985.
- 26 I. Bâldea, *Comment on “A single level tunneling model for molecular junctions: evaluating the simulation methods” by Opodi et al*, chemrxiv, DOI 10.26434/chemrxiv-2023-7fx77, 2023.
- 27 Y. Meir and N. S. Wingreen, *Phys. Rev. Lett.*, 1992, **68**, 2512–2515.
- 28 H. J. W. Haug and A.-P. Jauho, *Quantum Kinetics in Transport and Optics of Semiconductors*, Springer Series in Solid-State Sciences, Berlin, Heidelberg, New York, second, substantially revised edn., 2008, vol. 123.
- 29 L. A. Zotti, T. Kirchner, J.-C. Cuevas, F. Pauly, T. Huhn, E. Scheer and A. Erbe, *Small*, 2010, **6**, 1529–1535.
- 30 J. C. Cuevas and E. Scheer, *Molecular Electronics: An Introduction to Theory and Experiment*, World Scientific, 2nd edn., 2017.
- 31 C. Caroli, R. Combescot, P. Nozieres and D. Saint-James, *J. Phys. C: Solid State Phys.*, 1971, **4**, 916.
- 32 F. Zahid, M. Paulsson and S. Datta, in *Advanced Semiconductors and Organic Nano-Techniques*, ed. H. Morkoç, Academic Press, 2003, vol. 3, ch. Electrical Conduction through Molecules.
- 33 A. Sommerfeld and H. Bethe, in *Handbuch der Physik*, ed. Geiger and Scheel, Julius-Springer-Verlag, Berlin, 1933, vol. 24 (2), p. 446.
- 34 N. W. Ashcroft and N. D. Mermin, *Solid State Physics*, Saunders College Publishing, New York, 1976, pp. 20–23, 52.
- 35 E. Jahnke and F. Emde, *Tables of Functions with Formulae and Curves*, Dover Publications, fourth edition edn., 1945.
- 36 *Handbook of Mathematical Functions with Formulas, Graphs, and Mathematical Tables.*, ed. M. Abramowitz and I. A. Stegun, National Bureau of Standards Applied Mathematics Series, U.S. Government Printing Office, Washington, D.C., 1964.
- 37 I. Bâldea, *Adv. Theor. Simul.*, 2022, **5**, 2200077.
- 38 B. M. Briechle, Y. Kim, P. Ehrenreich, A. Erbe, D. Sysoiev, T. Huhn, U. Groth and E. Scheer, *Beilstein J. Nanotechnol.*, 2012, **3**, 798–808.
- 39 K. Luka-Guth, S. Hamsch, A. Bloch, P. Ehrenreich, B. M. Briechle, F. Kilibarda, T. Sandler, D. Sysoiev, T. Huhn, A. Erbe and E. Scheer, *Beilstein J. Nanotechnol.*, 2016, **7**, 1055–1067.
- 40 S. Guo, G. Zhou and N. Tao, *Nano Lett.*, 2013, **13**, 4326–4332.
- 41 Z. Xie, I. Bâldea and C. D. Frisbie, *J. Am. Chem. Soc.*, 2019, **141**, 3670–3681.
- 42 Z. Xie, I. Bâldea and C. D. Frisbie, *J. Am. Chem. Soc.*, 2019, **141**, 18182–18192.
- 43 Q. V. Nguyen, Z. Xie and C. D. Frisbie, *J. Phys. Chem. C*, 2021, **125**, 4292–4298.
- 44 Z. Xie, V. Diez Cabanes, Q. Van Nguyen, S. Rodriguez-Gonzalez, L. Norel, O. Galangau, S. Rigaut, J. Cornil and C. D. Frisbie, *ACS Applied Materials & Interfaces*, 2021, **13**, 56404–56412.
- 45 M.-W. Gu, H. H. Peng, I.-W. P. Chen and C.-h. Chen, *Nat. Mater.*, 2021, **20**, 658–664.
- 46 Y. Liu, X. Qiu, S. Soni and R. C. Chiechi, *Chemical Physics Reviews*, 2021, **2**, 021303.
- 47 B. Kim, S. H. Choi, X.-Y. Zhu and C. D. Frisbie, *J. Am. Chem. Soc.*, 2011, **133**, 19864–19877.

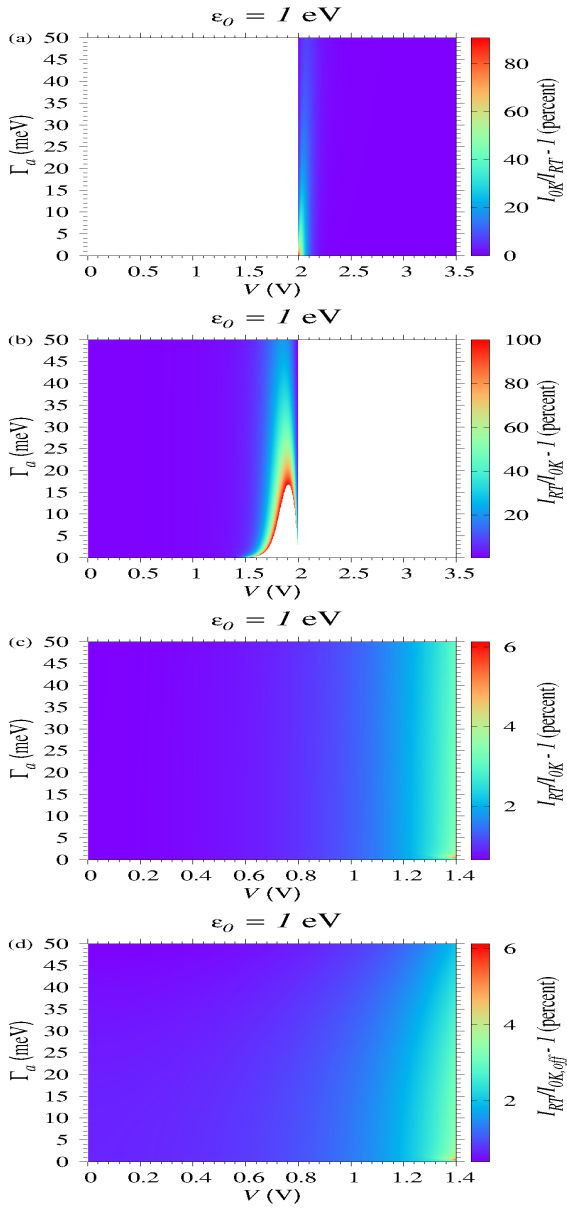


Fig. 1 The colored regions in the plane (V, Γ_a) depict situations where, at the fixed value of the MO energy offset indicated ($\epsilon_0 = 1$ eV), the current I_{0K} computed at $T = 0$ using eqn (3) is larger ($|eV| > 2|\epsilon_0|$, panel a) or smaller ($|eV| < 2|\epsilon_0|$, panel b) than the exact current I_{RT} computed from eqn (1) at room temperature ($T = 298.15$ K). For parameter values compatible with eqn (10), the current $I_{0K,off}$ computed using eqn (9) is very accurate (panel d); it is as accurate as I_{0K} (panel c). Relative deviations (shown only when not exceeding 100%) are indicated in the color box. To facilitate comparison between $I_{0K,off}$ and I_{0K} , abscissas in panel c depicting I_{0K} are restricted to those in panel d. Notice that the z -range in panels c and d is different from panel b.

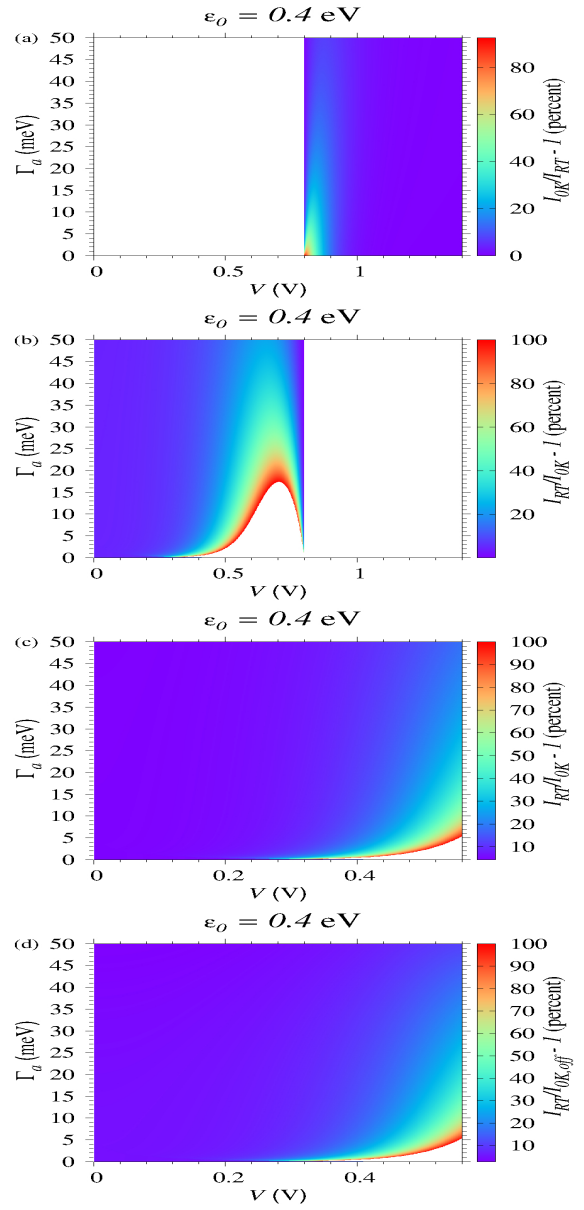


Fig. 2 The colored regions in the plane (V, Γ_a) depict situations where, at the fixed value of the MO energy offset indicated ($\epsilon_0 = 0.4$ eV), the current I_{0K} computed at $T = 0$ using eqn (3) is larger ($|eV| > 2|\epsilon_0|$, panel a) or smaller ($|eV| < 2|\epsilon_0|$, panel b) than the exact current I_{RT} computed from eqn (1) at room temperature ($T = 298.15$ K). For parameter values compatible with eqn (10) and (11), the current $I_{0K,off}$ computed using eqn (9) (panel d) is as accurate as I_{0K} (panel c). Relative deviations (shown only when not exceeding 100%) are indicated in the color box. To facilitate comparison between $I_{0K,off}$ and I_{0K} , abscissas in panel c depicting I_{0K} are restricted to those in panel d. Notice that the z -range in panels c and d is different from panel b.

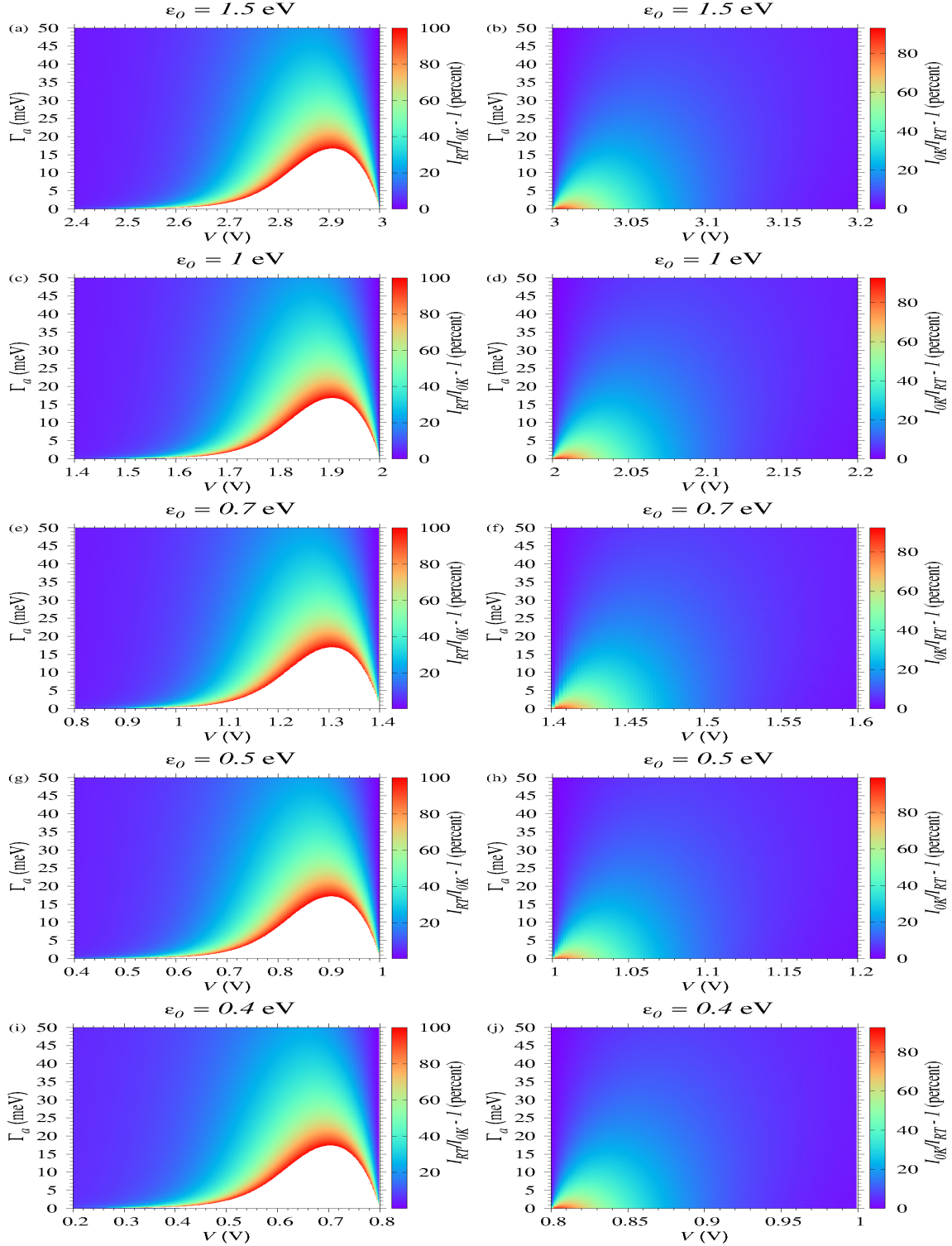


Fig. 3 For biases below resonance ($|eV| < 2|\epsilon_0|$, left panels), thermal effects enhance the room temperature I_{RT} (eqn (1)) with respect to the zero-temperature current I_{0K} (eqn (3)), while slightly reducing it ($I_{RT} < I_{0K}$) above resonance ($|eV| > 2|\epsilon_0|$, right panels). For sufficiently large values of $|\epsilon_0|$ ($\gtrsim 0.4$ eV), the location around resonance ($|eV| = 2|\epsilon_0|$) of the regions of the (V, Γ_a) -plane affected is nearly independent of ϵ_0 . Notice that all rightmost (leftmost) positions of the left (right) panels are aligned to resonance. In the white (empty) regions of the left panels the relative deviations exceed 100%.

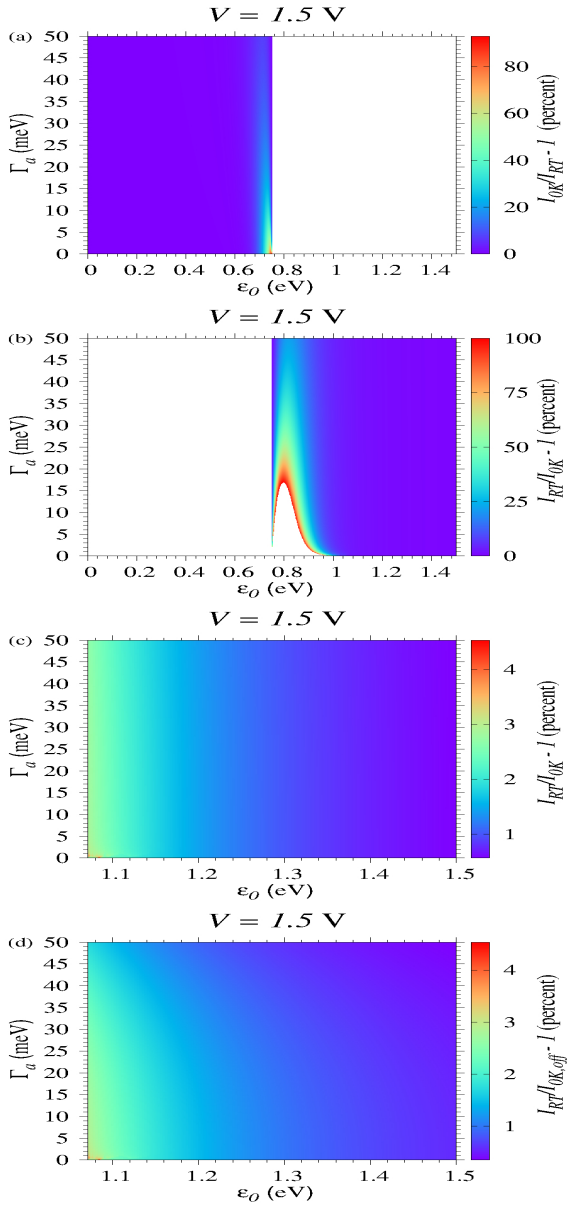


Fig. 4 The colored regions in the plane (ϵ_0, Γ_a) depict situations where, at the fixed bias indicated ($V = 1.5$ V), the current I_{0K} computed at $T = 0$ using eqn (3) is larger ($|eV| > 2|\epsilon_0|$, panel a) or smaller ($|eV| < 2|\epsilon_0|$, panel b) than the exact current I_{RT} computed from eqn (1) at room temperature ($T = 298.15$ K). For parameter values compatible with eqn (10), the current $I_{0K,off}$ computed using eqn (9) is very accurate (panel d); it is as accurate as I_{0K} (panel c). Relative deviations (shown only when not exceeding 100%) are indicated in the color box. To facilitate comparison between $I_{0K,off}$ and I_{0K} , abscissas in panel c depicting I_{0K} are restricted to those in panel d. Notice that the z -range in panels c and d is different from panel b.

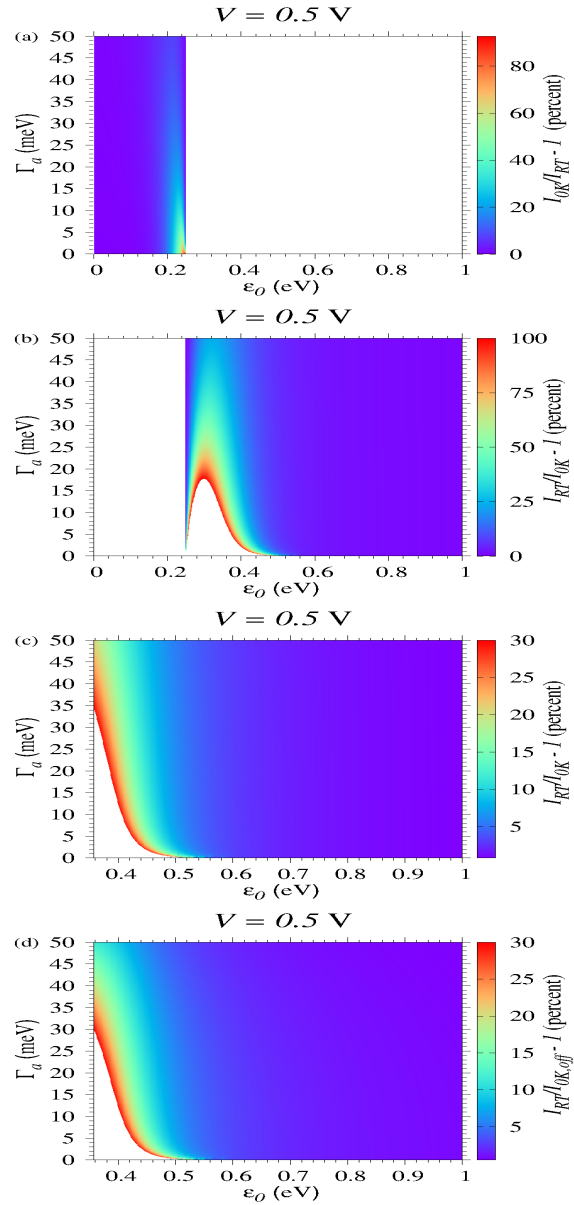


Fig. 5 The colored regions in the plane (ϵ_0, Γ_a) depict situations where, at the fixed bias indicated ($V = 0.5$ V), the current I_{0K} computed at $T = 0$ using eqn (3) is larger ($|eV| > 2|\epsilon_0|$, panel a) or smaller ($|eV| < 2|\epsilon_0|$, panel b) than the exact current I_{RT} computed from eqn (1) at room temperature ($T = 298.15$ K). For parameter values compatible with eqn (10) and (11), the current $I_{0K,off}$ computed using eqn (9) (panel d) is as accurate as I_{0K} (panel c). Relative deviations (shown only when not exceeding 100%) are indicated in the color box. To facilitate comparison between $I_{0K,off}$ and I_{0K} , abscissas in panel c depicting I_{0K} are restricted to those in panel d. Notice that the z -range in panels c and d is different from panel b.

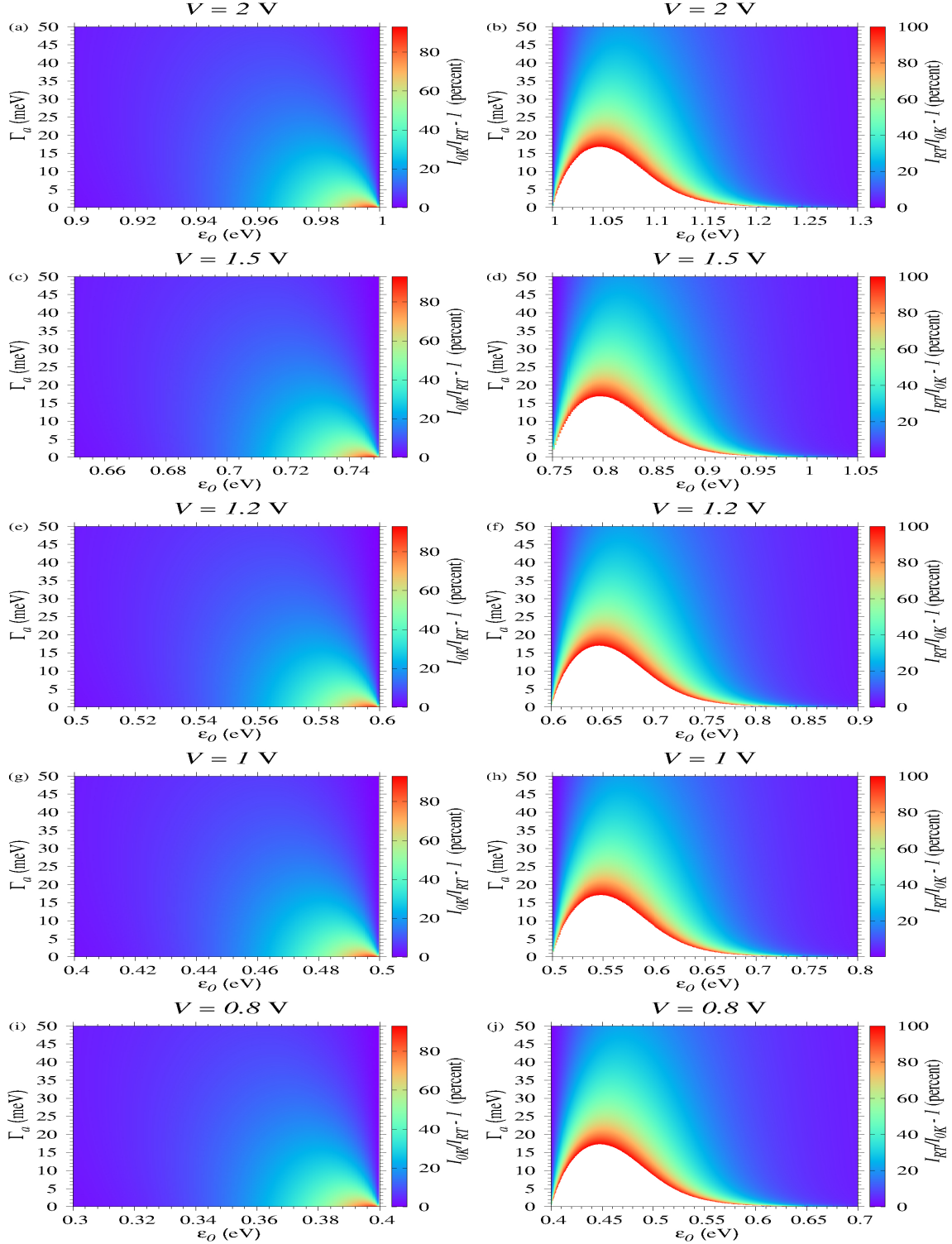


Fig. 6 Below resonance ($|eV| < 2|\epsilon_0|$, right panels), thermal effects enhance the room temperature current I_{RT} (eqn (1)) with respect to the zero-temperature current I_{0K} (eqn (3)), while slightly reducing it ($I_{RT} < I_{0K}$) above resonance ($|eV| > 2|\epsilon_0|$, left panels). For sufficiently large values of $|V|$ ($\gtrsim 0.8$ V), the location around resonance ($|eV| = 2|\epsilon_0|$) of the regions of the (ϵ_0, Γ_a) -plane affected is nearly independent of V . Notice that all rightmost (leftmost) positions of the left (right) panels are aligned to resonance. In the white (empty) regions of the left panels the relative deviations exceed 100%.

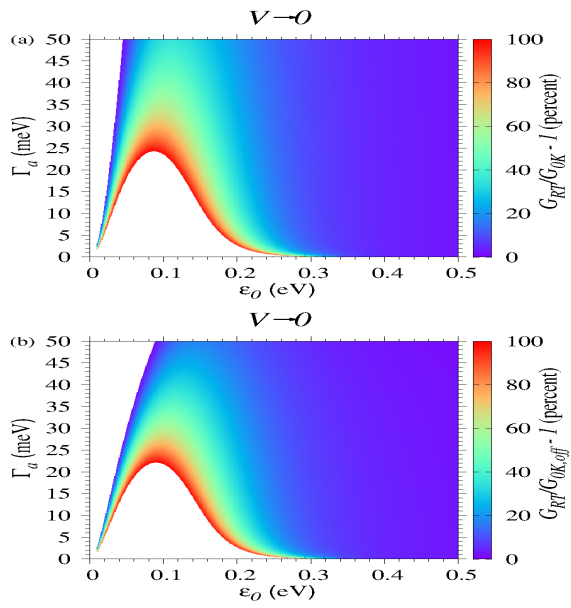


Fig. 7 Deviations in percent from the exact zero bias conductance $G_{exact} = G_{RT}$ computed exactly at $T = 298.15$ K (eqn (6)) of the ohmic conductance (a) G_{0K} and (b) $G_{0K,off}$ computed at $T = 0$ using eqn (5) and (12), respectively. Unless eqn (11) (see upper left corner), $G_{0K,off}$ is as accurate as G_{0K} .

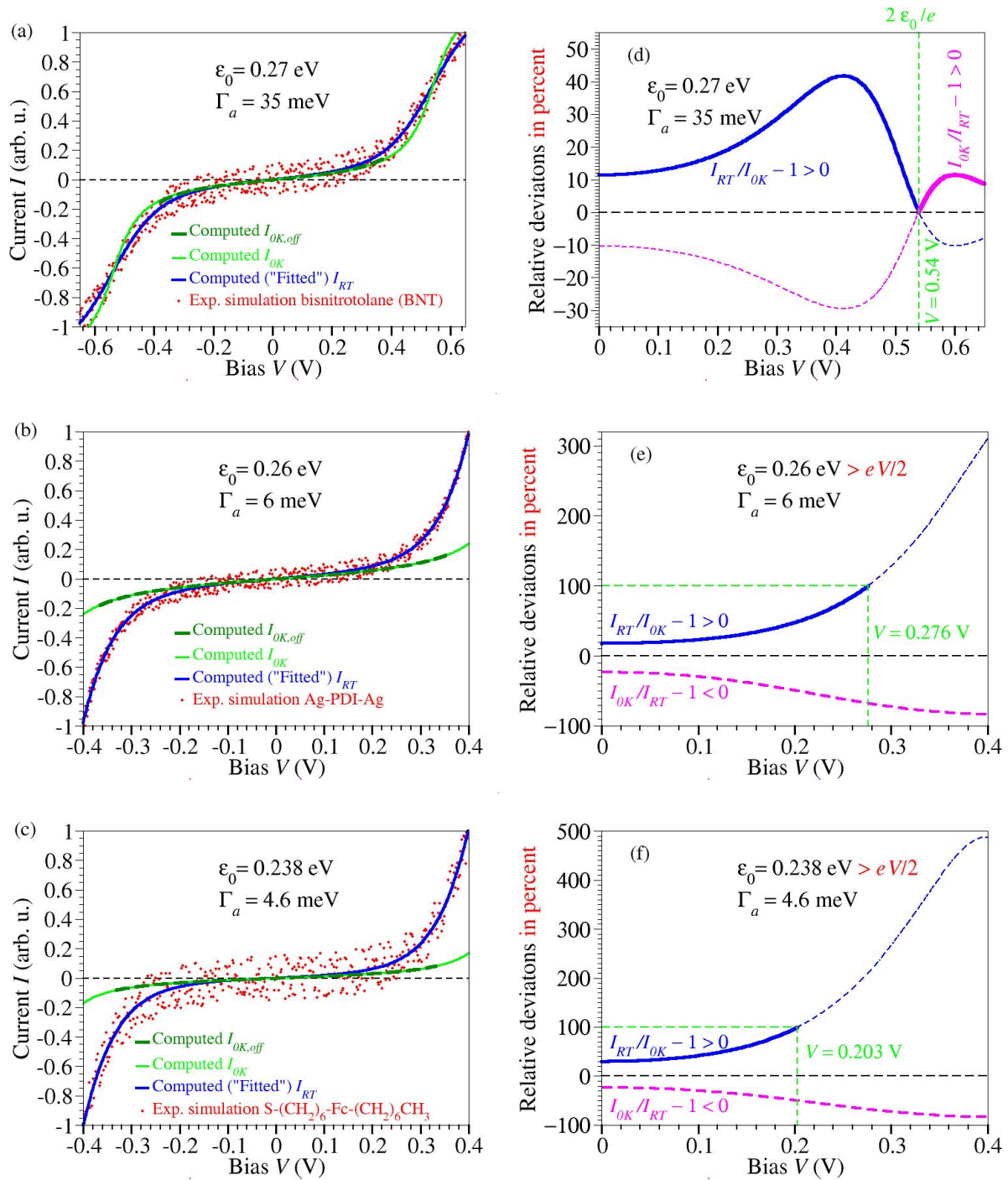


Fig. 8 Numerical simulations using literature model parameters^{21,25,29} for (a, d) single-molecule BNT junctions²⁹, (b, e) CP-AFM PDI junctions²¹, and (c, f) large-area junctions with EGaIn electrodes based on molecules of alkanethiolates functionalized with a ferrocene (Fc)¹⁷. Notwithstanding the similar values of the dominant MO energy offset ϵ_0 , the much larger value of the MO width Γ_a for BNT junctions makes the impact of temperature on current much weaker than for the other two junctions.

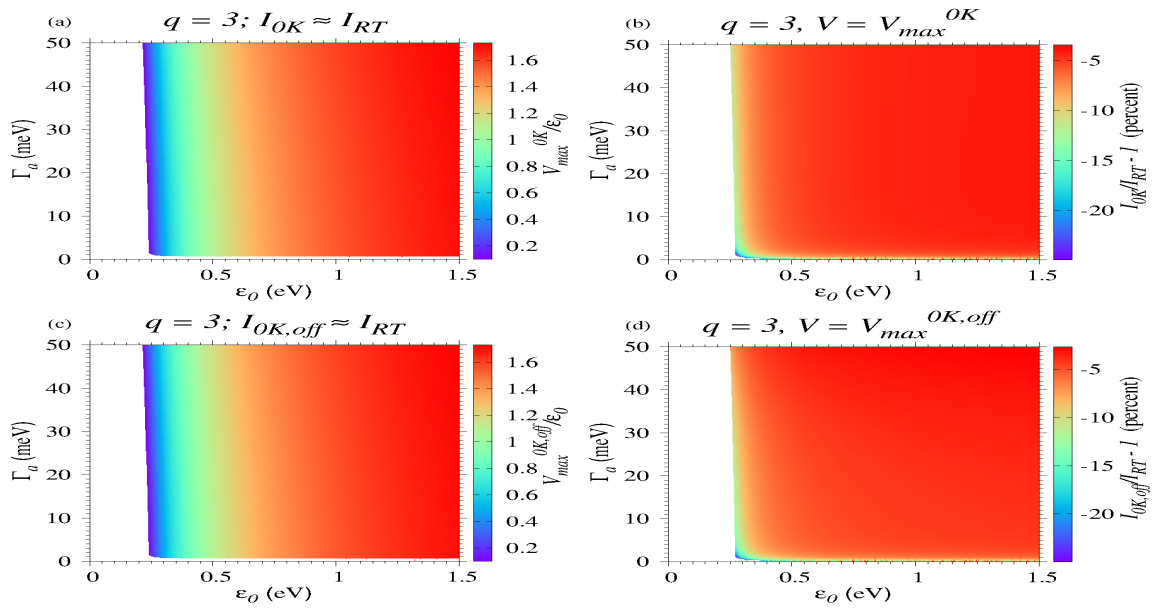


Fig. 9 The highest bias V_{max}^{OK} and $V_{max}^{OK,off}$ (panels a and b, respectively) at which eqn (3) and eqn (9) can reliably be applied for room temperature data processing. V_{max}^{OK} and $V_{max}^{OK,off}$ were computed from eqn (17a) and eqn (18b), respectively. They correspond to setting $q = 3$ in eqn (13b). The pertaining thermal corrections are presented in panels b and d, respectively.

Supplementary Information

Can room temperature data for tunneling molecular junctions be analyzed within a theoretical framework assuming zero temperature?

Ioan Bâldea ^{a*}

Keywords: molecular electronics, nanojunctions, single level model, thermal effects

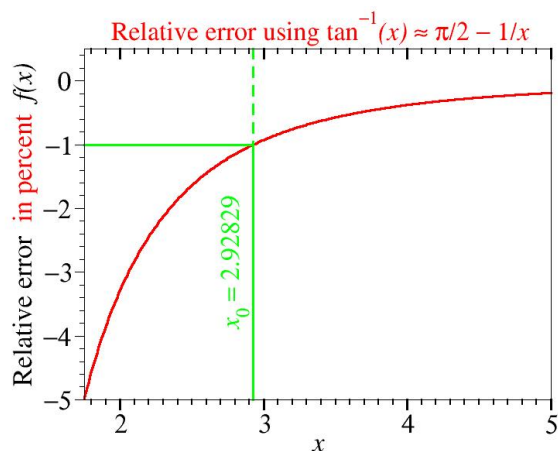


Fig. S1 Function $f(x) \equiv 100[(\pi/2 - 1/x)/\tan^{-1}x - 1]$ visualizing that the relative error in percent implied by using eqn (8a) is negligible.

^a Theoretical Chemistry, Heidelberg University, Im Neuenheimer Feld 229, D-69120 Heidelberg, Germany

* E-mail: ioan.baldea@pci.uni-heidelberg.de

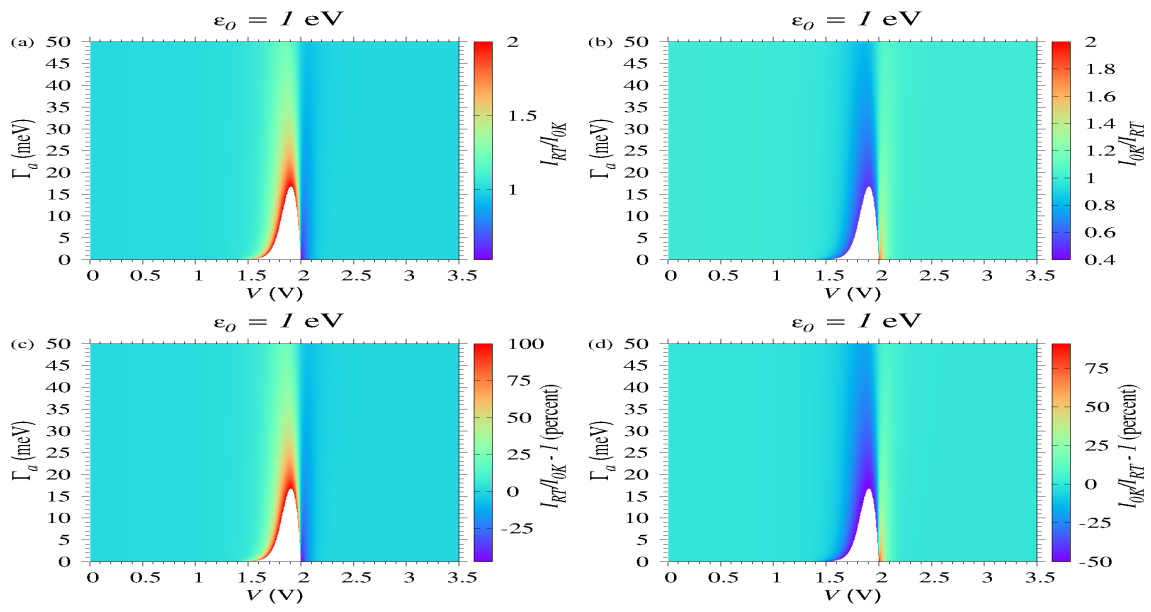


Fig. S2 Basically, the information presented in this figure on the deviations of the current I_{0K} computed at zero temperature using eqn (3) from the room temperature I_{RT} computed via eqn (1) is the same as that of Fig. 1a and b. We prefer the latter manner of presentation because we find it is easier to understand.

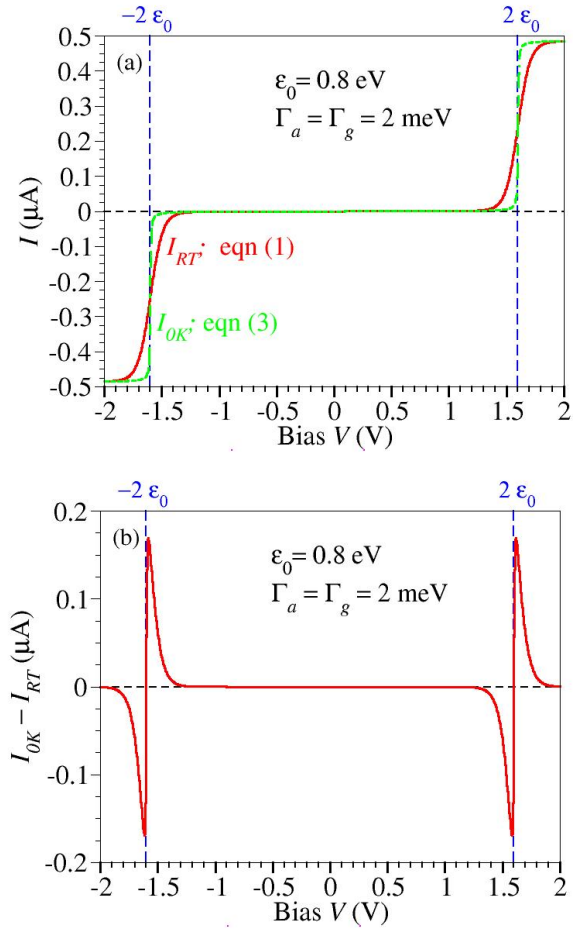


Fig. S3 (a) I - V curves computed using eqn (1) and eqn (3) illustrating that the thermal effect (b) enhances the current below resonance ($|I_{RT}| > |I_{0K}|$ for $|eV| < 2|\varepsilon_0|$) while reducing it above resonance ($|I_{RT}| < |I_{0K}|$ for $|eV| > 2|\varepsilon_0|$).

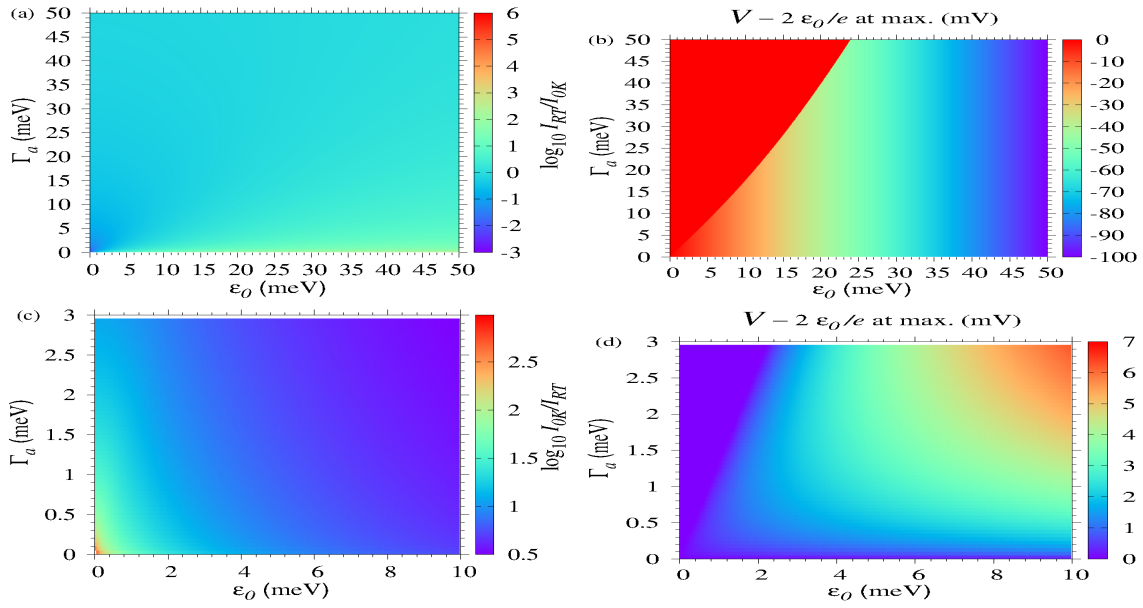


Fig. S4 Results at very small values of the MO offset ϵ_0 showing an opposite behavior to that at (reasonably) large ϵ_0 . Panel (a) depicts situations below resonance wherein $I_{RT} < I_{0K}$. Likewise, panel c shows situations above resonance wherein $I_{0K} < I_{RT}$. The values of panel a (panel c) were computed at the biases V_m that maximize the ratio I_{RT}/I_{0K} (I_{0K}/I_{RT}). The corresponding differences from resonance $V_m - 2\epsilon_0/e$ are presented in panels b and d, respectively.

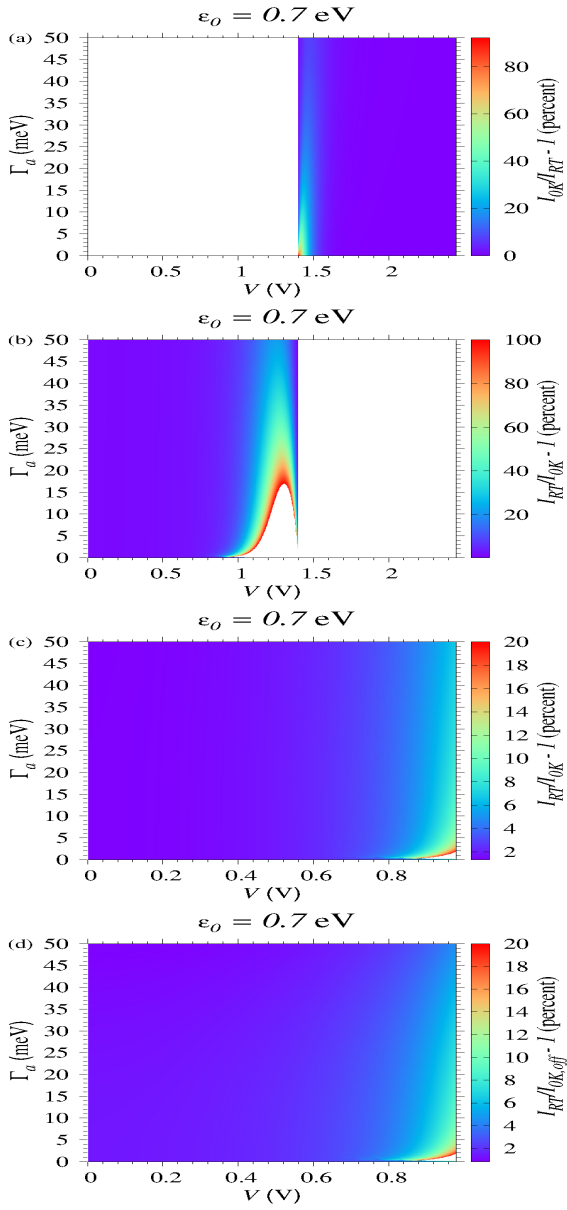


Fig. S5 The colored regions in the plane (V, Γ_d) depict situations where, at the fixed value of the MO energy offset indicated ($\epsilon_0 = 0.7$ eV), the current I_{0K} computed at $T = 0$ using eqn (3) is larger ($|eV| > 2|\epsilon_0|$, panel a) or smaller ($|eV| < 2|\epsilon_0|$, panel b) than the exact current I_{RT} computed from eqn (1) at room temperature ($T = 298.15$ K). For parameter values compatible with eqn (10) and (11), the current $I_{0K,off}$ computed using eqn (9) is very accurate (panel d); it is as accurate as I_{0K} (panel c). Relative deviations (shown only when not exceeding 100%) are indicated in the color box. To facilitate comparison between $I_{0K,off}$ and I_{0K} , abscissas in panel c depicting I_{0K} are restricted to those in panel d. Notice that the z -range in panels (c) and (d) is different from panel b.

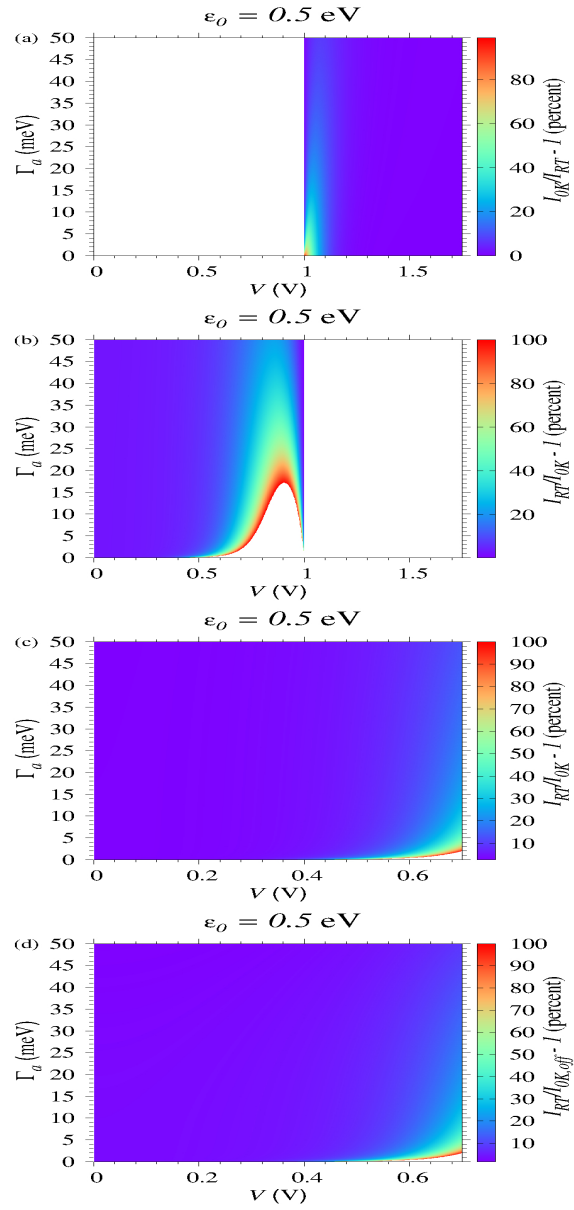


Fig. S6 The colored regions in the plane (V, Γ_d) depict situations where, at the fixed value of the MO energy offset indicated ($\epsilon_0 = 0.5$ eV), the current I_{0K} computed at $T = 0$ using eqn (3) is larger ($|eV| > 2|\epsilon_0|$, panel a) or smaller ($|eV| < 2|\epsilon_0|$, panel b) than the exact current I_{RT} computed from eqn (1) at room temperature ($T = 298.15$ K). For parameter values compatible with eqn (10) and (11), the current $I_{0K,off}$ computed using eqn (9) is very accurate (panel d); it is as accurate as I_{0K} (panel c). Relative deviations (shown only when not exceeding 100%) are indicated in the color box. To facilitate comparison between $I_{0K,off}$ and I_{0K} , abscissas in panel c depicting I_{0K} are restricted to those in panel d. Notice that the z -range in panels (c) and (d) is different from panel b.

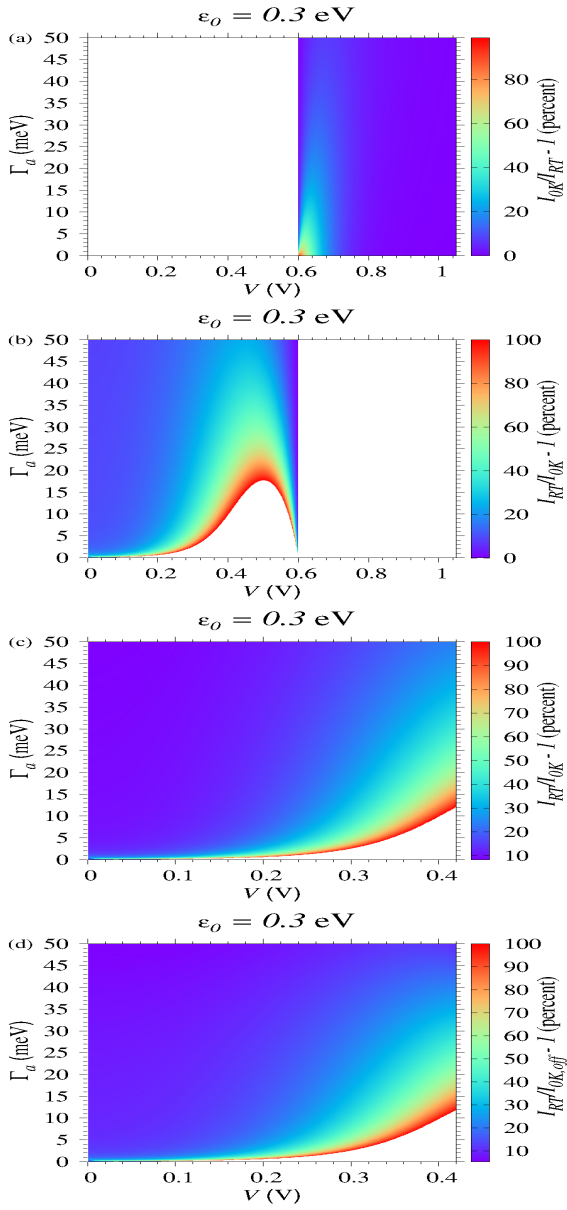


Fig. S7 The colored regions in the plane (V, Γ_a) depict situations where, at the fixed value of the MO energy offset indicated ($\epsilon_0 = 0.3$ eV), the current I_{0K} computed at $T = 0$ using eqn (3) is larger ($|eV| > 2|\epsilon_0|$, panel a) or smaller ($|eV| < 2|\epsilon_0|$, panel b) than the exact current I_{RT} computed from eqn (1) at room temperature ($T = 298.15$ K). For parameter values compatible with eqn (10) and (11), the current $I_{0K,off}$ computed using eqn (9) (panel d) is as accurate as I_{0K} (panel c). Relative deviations (shown only when not exceeding 100%) are indicated in the color box. To facilitate comparison between $I_{0K,off}$ and I_{0K} , abscissas in panel c depicting I_{0K} are restricted to those in panel d. Notice that the z -range in panels (c) and (d) is different from panel b.

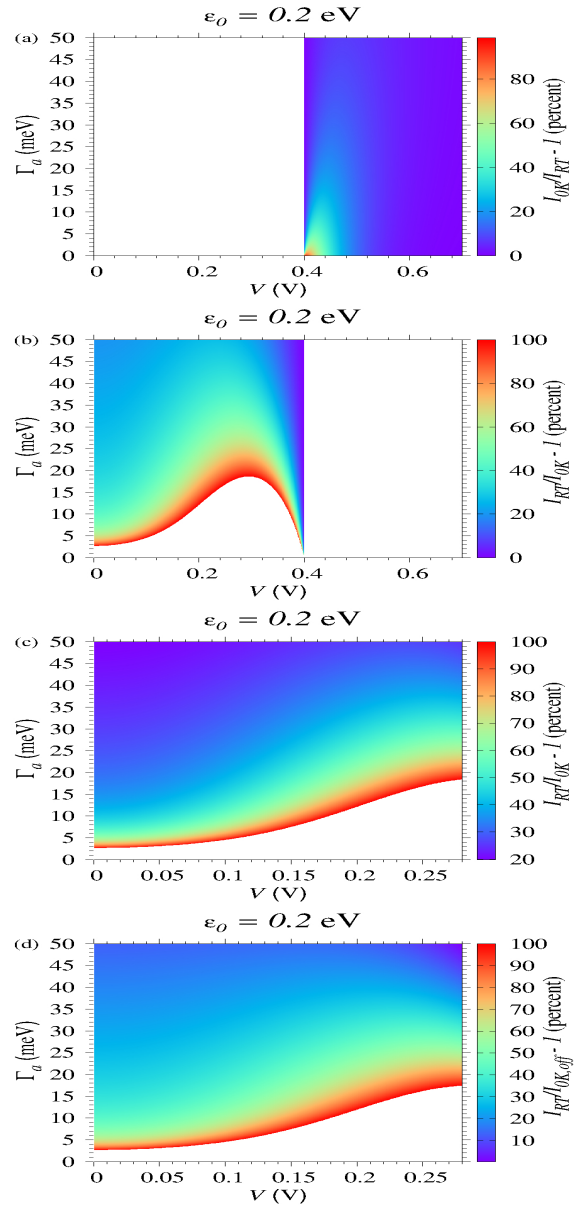


Fig. S8 The colored regions in the plane (V, Γ_a) depict situations where, at the fixed value of the MO energy offset indicated ($\epsilon_0 = 0.2$ eV), the current I_{0K} computed at $T = 0$ using eqn (3) is larger ($|eV| > 2|\epsilon_0|$, panel a) or smaller ($|eV| < 2|\epsilon_0|$, panel b) than the exact current I_{RT} computed from eqn (1) at room temperature ($T = 298.15$ K). For parameter values compatible with eqn (10) and (11), the current $I_{0K,off}$ computed using eqn (9) (panel d) is as accurate as I_{0K} (panel c). Relative deviations (shown only when not exceeding 100%) are indicated in the color box. To facilitate comparison between $I_{0K,off}$ and I_{0K} , abscissas in panel c depicting I_{0K} are restricted to those in panel d. Notice that the z -range in panels (c) and (d) is different from panel b.

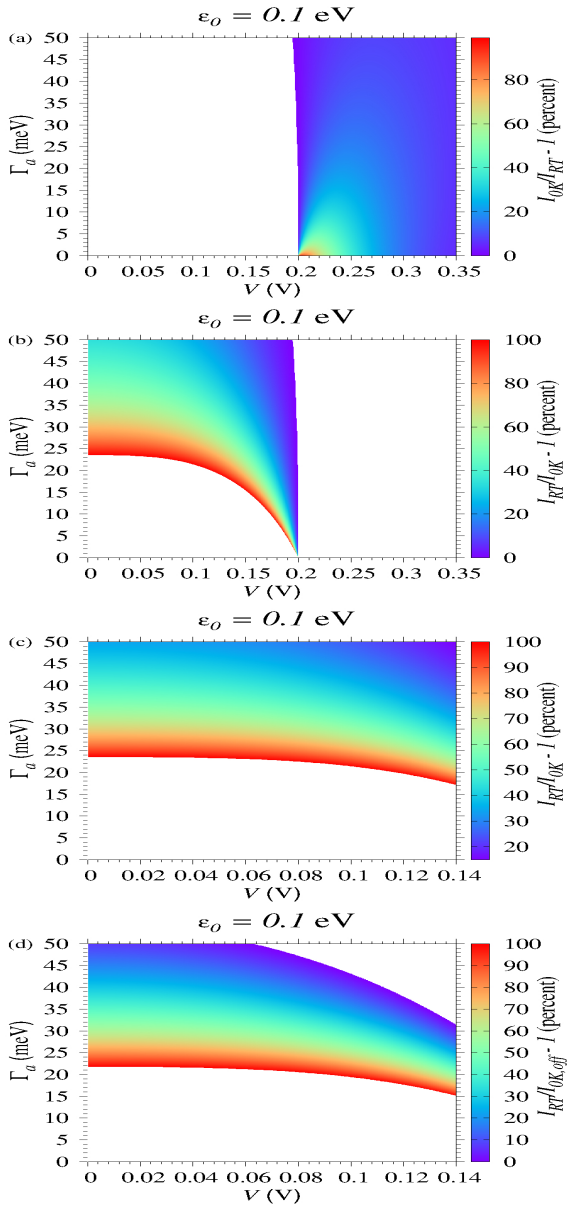


Fig. S9 The colored regions in the plane (V, Γ_d) depict situations where, at the fixed value of the MO energy offset indicated ($\epsilon_0 = 0.1$ eV), the current I_{0K} computed at $T = 0$ using eqn (3) is larger ($|eV| > 2|\epsilon_0|$, panel a) or smaller ($|eV| < 2|\epsilon_0|$, panel b) than the exact current I_{RT} computed from eqn (1) at room temperature ($T = 298.15$ K). For situations violating eqn (11), the current $I_{0K,off}$ computed using eqn (9) (panel d) stronger departs from I_{RT} than I_{0K} (panel d). Relative deviations (shown only when not exceeding 100%) are indicated in the color box. To facilitate comparison between $I_{0K,off}$ and I_{0K} , abscissas in panel c depicting I_{0K} are restricted to those in panel d. Notice that the z -range in panels (c) and (d) is different from panel b.

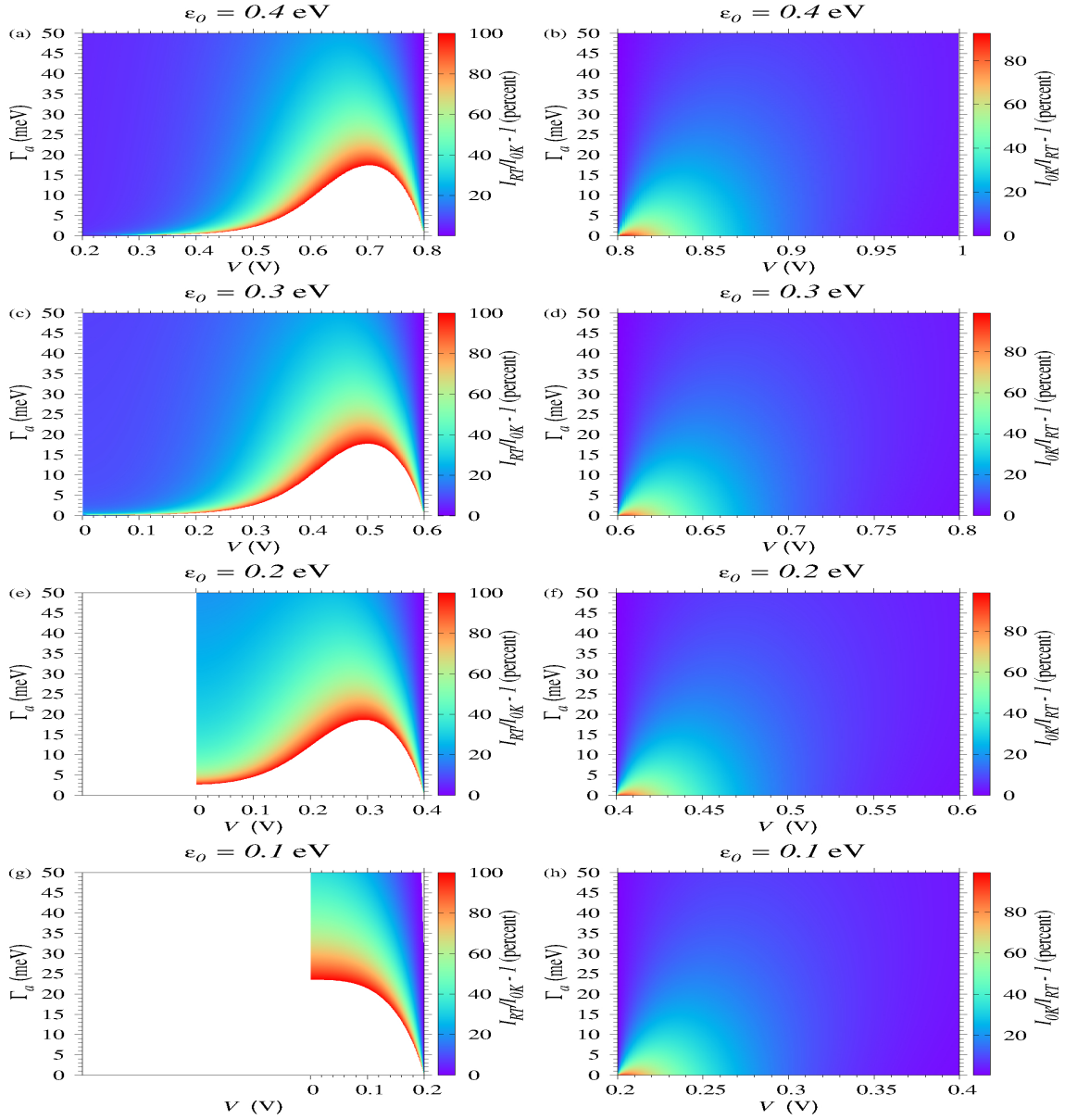


Fig. S10 Results for lower biases illustrating the current enhancement below resonance ($|eV| < 2|\epsilon_0|$, left panels) and current reduction above resonance ($|eV| > 2|\epsilon_0|$, right panels). As ϵ_0 decreases (downwards), the white (empty) region (wherein the relative deviations exceed 100%) in the left panels extends upwards to larger Γ_a and comprises a broader bias range. Notice that all rightmost (leftmost) positions of the left (right) panels are aligned to resonance.

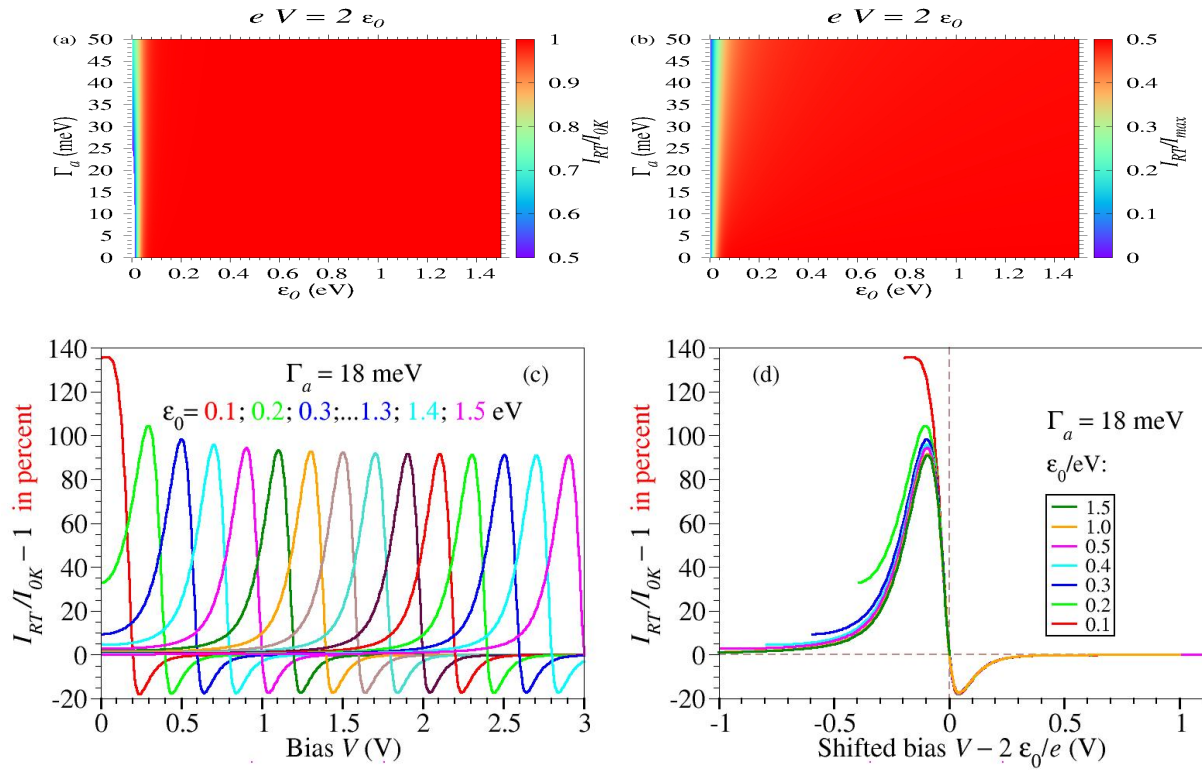


Fig. S11 (a,b) Strictly on resonance, the temperature impact on the current is negligible. (c,d) Except for small values of the MO energy offset ϵ_0 , the thermal enhancement of the current occurs around resonance and is quite insensitive to ϵ_0 .

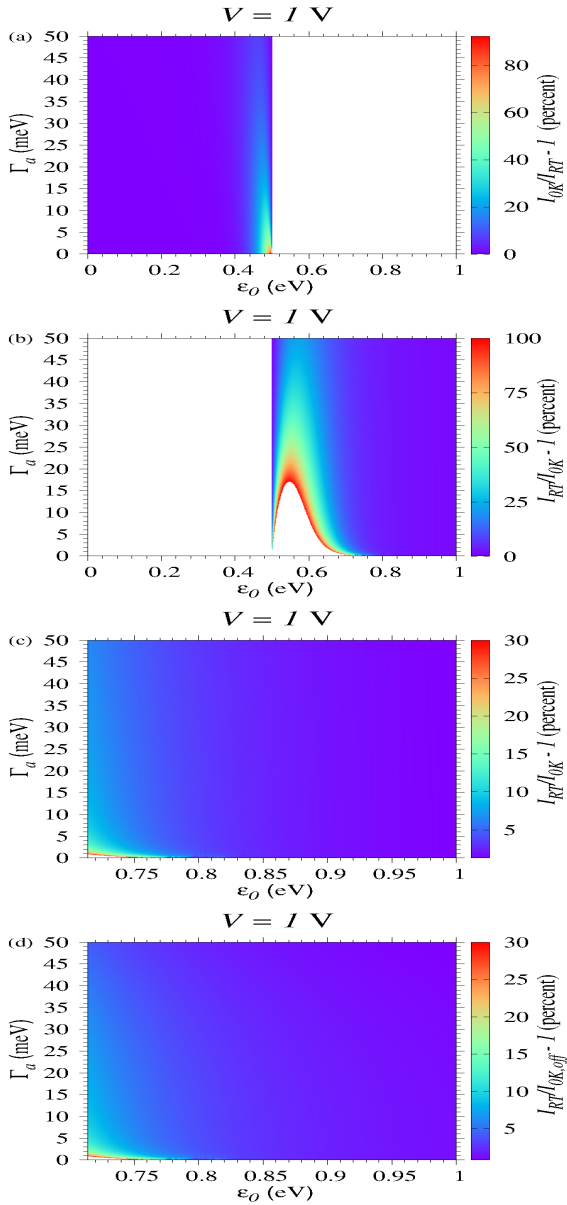


Fig. S12 The colored regions in the plane (ϵ_0, Γ_a) depict situations where, at the fixed bias indicated ($V = 1$ V), the current I_{0K} computed at $T = 0$ using eqn (3) is larger ($|eV| > 2|\epsilon_0|$, panel a) or smaller ($|eV| < 2|\epsilon_0|$, panel b) than the exact current I_{RT} computed from eqn (1) at room temperature ($T = 298.15$ K). For parameter values compatible with eqn (10) and (11), the current $I_{0K,off}$ computed using eqn (9) is very accurate (panel d); it is as accurate as I_{0K} (panel c). Relative deviations (shown only when not exceeding 100%) are indicated in the color box. To facilitate comparison between $I_{0K,off}$ and I_{0K} , abscissas in panel c depicting I_{0K} are restricted to those in panel d. Notice that the z -range in panels (c) and (d) is different from panel b.

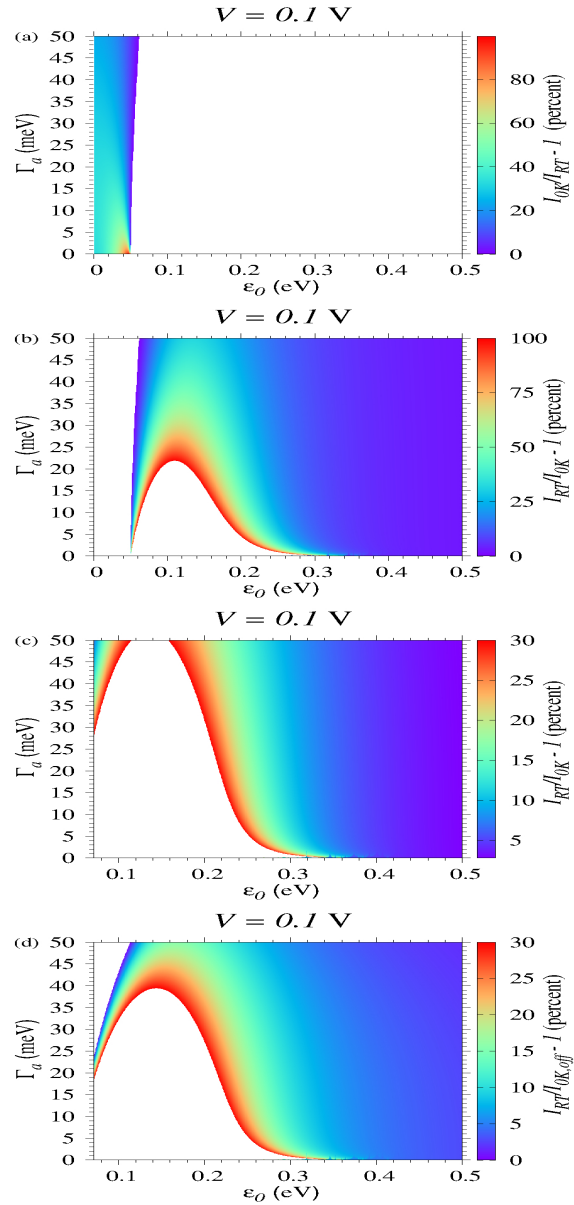


Fig. S13 The colored regions in the plane (ϵ_0, Γ_a) depict situations where, at the fixed bias indicated ($V = 0.1$ V), the current I_{0K} computed at $T = 0$ using eqn (3) is larger ($|eV| > 2|\epsilon_0|$, panel a) or smaller ($|eV| < 2|\epsilon_0|$, panel b) than the exact current I_{RT} computed from eqn (1) at room temperature ($T = 298.15$ K). The fact that in this case, paradoxically, the current $I_{0K,off}$ computed using eqn (9) (panel d) is closer to I_{RT} than I_{0K} (panel c) is an error compensation effect. Relative deviations (shown only when not exceeding 100%) are indicated in the color box. To facilitate comparison between $I_{0K,off}$ and I_{0K} , abscissas in panel c depicting I_{0K} are restricted to those in panel d. Notice that the z -range in panels (c) and (d) is different from panel b.

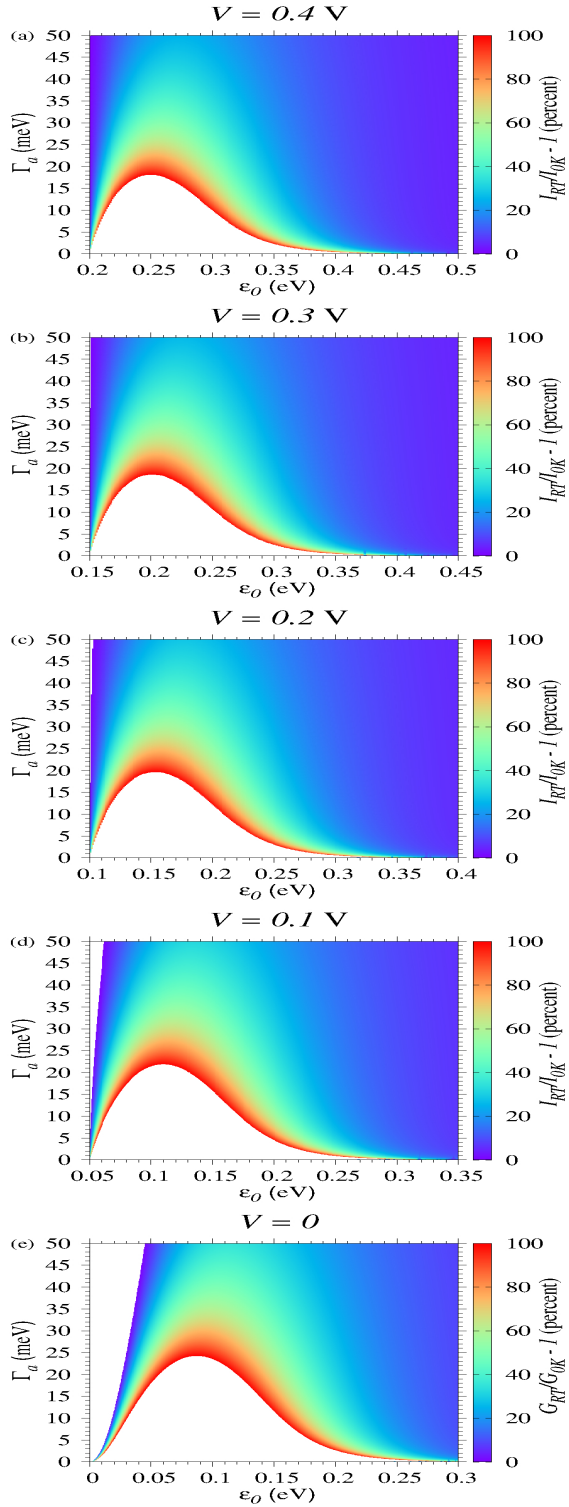


Fig. S14 Results illustrating the current enhancement below resonance ($|eV| < 2|\epsilon_0|$) at lower biases. As the bias decreases (downwards), the white (empty) region (wherein the relative deviations exceed 100%) extends upwards to larger Γ_a and comprises a broader ϵ_0 -range. Notice that the leftmost positions of all panels are aligned to resonance.

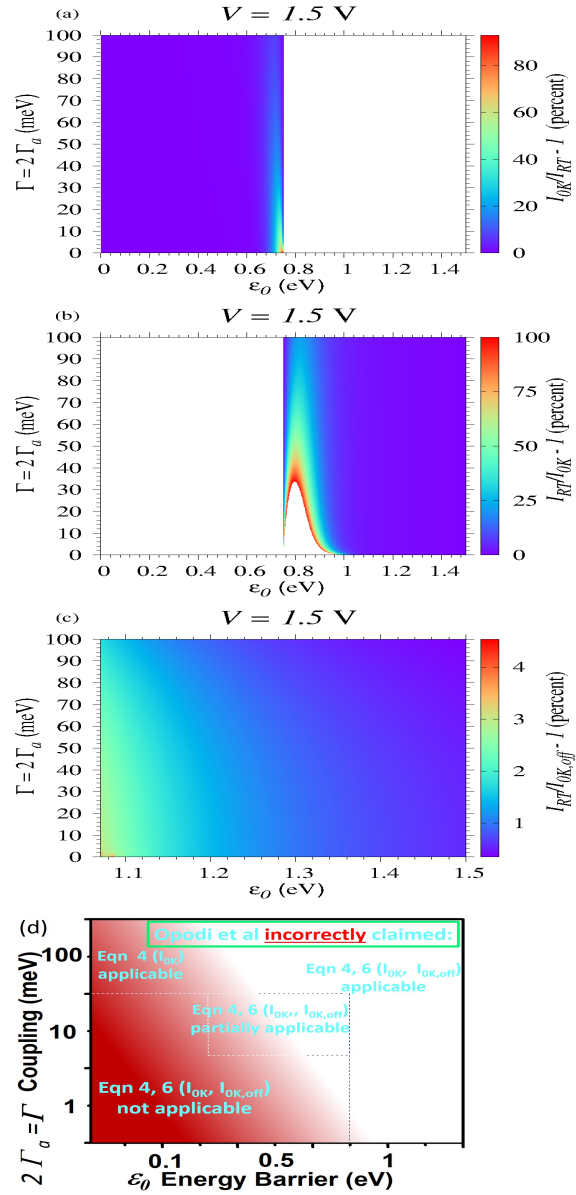


Fig. S15 Relative deviations in percent of the currents I_{0K} (panel a and b) and $I_{0K,off}$ (panel c) computed via eqn (3) and (9) assuming zero temperature from the exact current I_{RT} computed at room temperature. Comparison with panel d (adapted from Opodi et al, Phys. Chem. Chem. Phys. 2022, 24, 11958 and ref. 26) demonstrates that Fig. 5 of Opodi et al is a factual error. Notice that, in order to facilitate comparison with the paper by Opodi et al, the electronic coupling $\Gamma = 2\Gamma_a$ in panel d is different from Fig. 4.

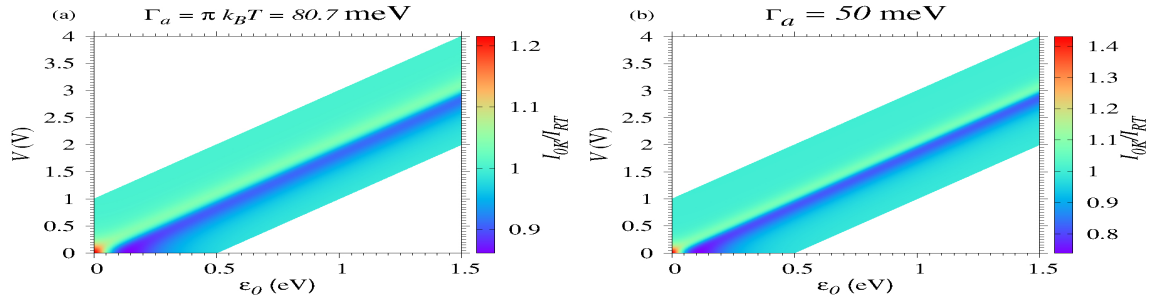


Fig. S16 Panel b visualizes the weak impact of the (room) temperature on the current at the highest value $\Gamma_a = 50$ meV chosen in most diagrams, which is even smaller than the value $\Gamma_a = \pi k_B T_{RT} = 80.7$ meV (panel a) where a weak temperature effect can be expected in view of eqn (13a).

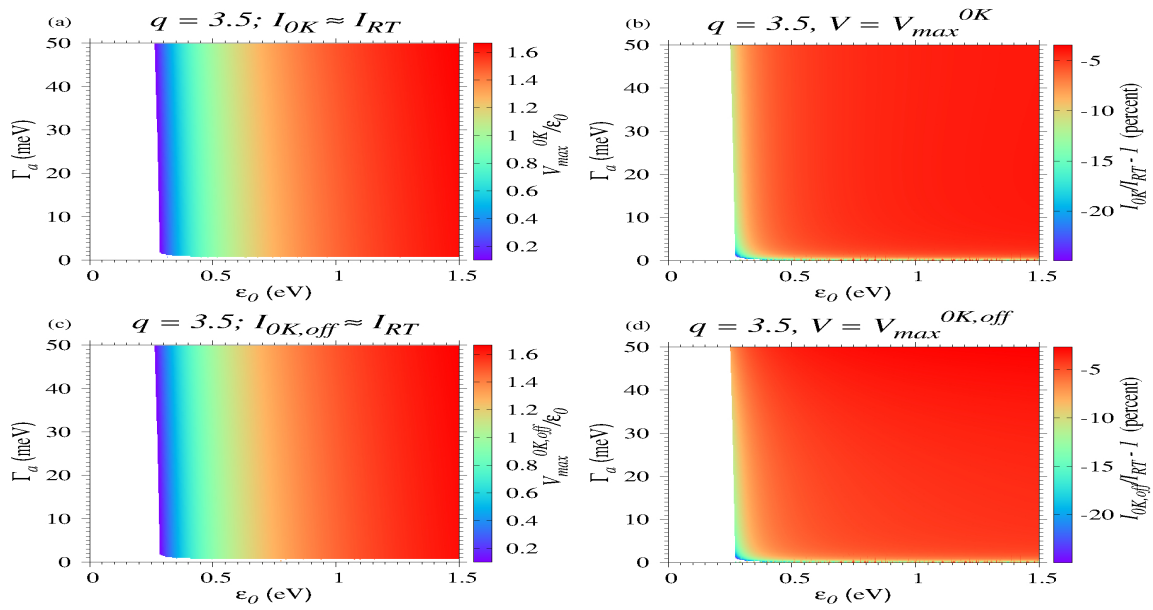


Fig. S17 Similar to Fig. 9 but setting $q = 3.5$ in eqn (13b).

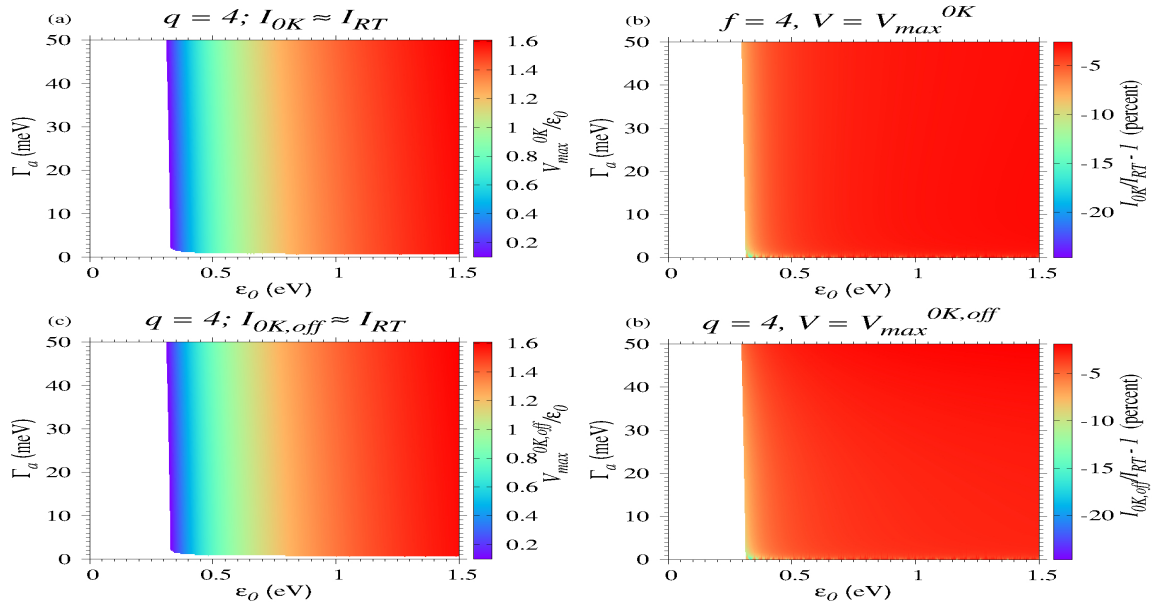


Fig. S18 Similar to Fig. 9 but setting $q = 4$ in eqn (13b).

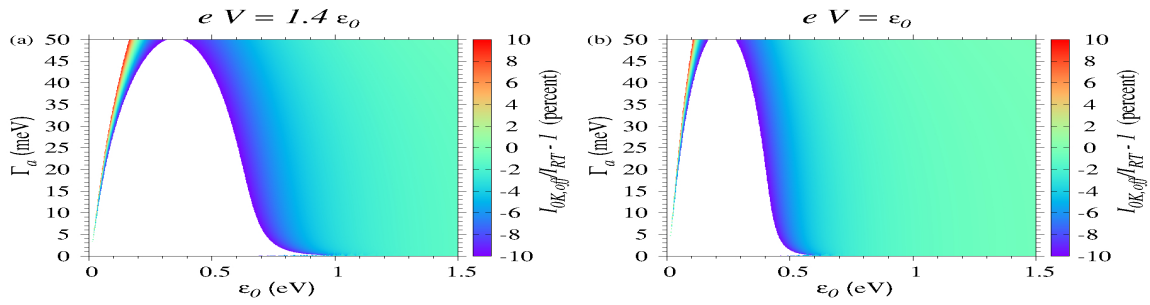


Fig. S19 This figure illustrates how restriction to the narrower bias range $|eV| < |\epsilon_0|$ (panel b) can render data fitting using $I_{OK,off}$ (eqn (9)) applicable for junctions having, e.g., $\epsilon_0 \simeq 0.5$ eV, a fact impossible when using the broader bias range $|eV| < 1.4 |\epsilon_0|$ (panel a).